

Few-body spin couplings and their implications for universal quantum computation

Ryan Woodworth¹, Ari Mizel^{1,2}, and Daniel A. Lidar³

¹*Physics Department and* ²*Materials Research Institute,*
Pennsylvania State University, University Park, PA 16802 and

³*Chemical Physics Theory Group, and Center for Quantum Information and Quantum Control,*
University of Toronto, 80 St. George St., Toronto, Ontario M5S 3H6, Canada

Electron spins in semiconductor quantum dots are promising candidates for the experimental realization of solid-state qubits. We analyze the dynamics of a system of three qubits arranged in a linear geometry and a system of four qubits arranged in a square geometry. Calculations are performed for several quantum dot confining potentials. In the three-qubit case, three-body effects are identified that have an important quantitative influence upon quantum computation. In the four-qubit case, the full Hamiltonian is found to include both three-body and four-body interactions that significantly influence the dynamics in physically relevant parameter regimes. We consider the implications of these results for the encoded universality paradigm applied to the four-electron qubit code; in particular, we consider what is required to circumvent the four-body effects in an encoded system (four spins per encoded qubit) by the appropriate tuning of experimental parameters.

PACS numbers: 03.67.Pp, 03.67.Lx, 75.10.Jm

INTRODUCTION

Electron spins in semiconductor quantum dots are a leading candidate for the physical realization of qubits in a quantum computer [1]. Although any quantum algorithm can be implemented using single-qubit and two-qubit gates [2], many such algorithms realize substantial increases in efficiency by exploiting simultaneous interactions among three or more qubits [3, 4, 5, 6, 7, 8, 9, 10, 11, 12, 13, 14, 15, 16]. In order to employ such simultaneous interactions, it is essential to understand in detail the many-body dynamics of the system of coupled qubits. More generally, since a practical quantum computer may need to contain as many as 10^6 qubits [3], it is essential to characterize the effect of many-body interactions on the system's overall energy landscape.

In past work [17], we used a model confining potential of superposed parabolic minima to demonstrate that three-body effects significantly influence the Hamiltonian of three electrons confined to three quantum dots at the vertices of an equilateral triangle and that four-body effects are significant for four electrons confined to a tetrahedral arrangement of four dots. Here we extend these results in two ways. First, we analyze three quantum dots in a linear geometry [18] and four dots in a square geometry [19] since these geometries are more likely to occur in a real quantum computer apparatus. Second, by employing a Gaussian shape for the confining potential of each well [20], we explore the sensitivity of the many-body effects to the form of the confining potential. In both cases, a non-perturbative calculation finds that many-body effects contribute appreciably to the Hamiltonian. We note that Scarola et al. [21, 22] have demonstrated that the application of a magnetic field allows chiral terms to arise in the spin Hamiltonian, which modifies this Hamiltonian in another important manner as compared to the naive

Heisenberg form.

To date, discussions of quantum dot quantum computation have nearly always assumed pairwise Heisenberg interactions. In view of the above result, this implies that computational errors may occur in the context of quantum computers using electron spin qubits in quantum dots, unless one always simultaneously couples only disjoint pairs of dots. There are at least four circumstances where this may be undesirable or even infeasible. One is fault tolerant quantum error correction, where simultaneous operations on several coupled dots have been associated with better error thresholds. A second is adiabatic quantum computation [11], in which the final Hamiltonian may include the simultaneous interactions that we discuss here. We will not analyze these possibilities here, although we believe that the methods we discuss below are relevant to them.

We will focus on two other contexts, that of “encoded universality” (EU) [5, 6, 7, 8, 9] and that of computation on decoherence-free subspaces (DFSs) [5, 6, 23] and supercoherent qubits [10]. In these cases, the goal is to perform universal quantum computation using (EU:) only the most easily controllable interaction, or (DFS, supercoherence:) using only interactions that preserve the code subspace, since that subspace offers protection against certain types of decoherence. (Strong and fast exchange interaction pulses can further be used to suppress decoherence [24] and to eliminate decoherence-induced leakage [25].)

We will refer to these cases collectively as “encoded quantum computation.” It turns out that universal quantum computation using only the Heisenberg exchange interaction is an extremely attractive possibility in encoded models, and we will consider it in detail below. After establishing that four-body interaction terms can arise in a Heisenberg exchange Hamiltonian, we in-

investigate the question of neutralizing their effect by using encoded qubits [5, 6, 8, 9, 10, 23, 24, 25, 26, 27, 28]. By generalizing the work of Bacon [29], who showed that universal quantum computation was possible using encoded gates with two-body coupling Hamiltonians (i.e., assuming that the Heisenberg Hamiltonian was applicable even when coupling three or more dots at a time), we enumerate tuning conditions on experimental parameters that are needed for the four-body effects to cancel out. An alternative is to design these encoded gates while allowing only pairs of electrons to couple at any given time. This is indeed possible, as shown in Ref. [30], for the price of significantly longer pulse sequences per given encoded gate. Nevertheless, in view of the findings reported here and in Refs. [21, 22], this price may be worth paying.

THREE-ELECTRON CASE USING A POLYNOMIAL POTENTIAL

A system of three electrons within a confining scalar potential $V(\mathbf{r})$ obeys the Hamiltonian

$$H = \sum_{i=1}^3 \left[\frac{\mathbf{p}_i^2}{2m} + V(\mathbf{r}_i) \right] + \sum_{i<j} \frac{e^2}{\kappa |\mathbf{r}_i - \mathbf{r}_j|} \quad (1)$$

$$\equiv \sum_{i=1}^3 h(\mathbf{r}_i) + \sum_{i<j} w(\mathbf{r}_i, \mathbf{r}_j) \quad (2)$$

in the absence of spin-orbit coupling and external magnetic fields. Following Ref. [17], we will first choose the confining potential $V(\mathbf{r}_i)$ to have the relatively simple form

$$V(\mathbf{r}) = \frac{1}{2(2l)^4} m\omega_o^2 |\mathbf{r} - \mathbf{A}|^2 |\mathbf{r} - \mathbf{B}|^2 |\mathbf{r} - \mathbf{C}|^2, \quad (3)$$

where the minima \mathbf{A} , \mathbf{B} , and \mathbf{C} are collinear and separated by a distance $2l$ (Fig. 1). We assume a Heitler-London approximation [31], wherein excited orbital states and states with double occupation of any single dot are neglected (see Ref. [22] for a recent discussion of the validity of this approximation in the context of electron spin qubits). The system's only degrees of freedom are therefore the spins of the confined electrons, leading to a total of $2^3 = 8$ “computational” basis states

$$|\Psi(s_A, s_B, s_C)\rangle = \sum_P \delta_P P[|A\rangle |B\rangle |C\rangle |s_A\rangle |s_B\rangle |s_C\rangle]. \quad (4)$$

In the above, $|\{A\}\rangle$ are the three localized orbital ground states; $|s_{\{A\}}\rangle$ denote the corresponding spin states; P is the set of all permutations of $\{A, B, C\}$; and δ_P is 1 (-1) for even (odd) permutations. For instance, one of the

eight (unnormalized) basis states is

$$\begin{aligned} |\Psi(\uparrow\uparrow\downarrow)\rangle &= |ABC\rangle |\uparrow\uparrow\downarrow\rangle - |ACB\rangle |\uparrow\downarrow\uparrow\rangle \\ &+ |CAB\rangle |\downarrow\uparrow\uparrow\rangle - |CBA\rangle |\downarrow\uparrow\uparrow\rangle \\ &+ |BCA\rangle |\uparrow\downarrow\uparrow\rangle - |BAC\rangle |\uparrow\uparrow\downarrow\rangle. \end{aligned}$$

To characterize the localized orbital state $|\{A\}\rangle$ for each dot, we solve the Schrödinger equation as though the other potential wells were absent:

$$\phi_A(\mathbf{r}) \equiv \langle \mathbf{r} | A \rangle \equiv \left(\frac{m\omega_o}{\pi\hbar} \right)^{3/4} \exp \left(-\frac{m\omega_o}{2\hbar} |\mathbf{r} - \mathbf{A}|^2 \right) \quad (5)$$

(Fig. 2). Because these orbitals overlap at least slightly for any finite ω_o , the states (4) are not orthogonal.

We now define H_{spin} to be the matrix representation of H in the basis (4), and expand it in terms of tensor products of Pauli matrices:

$$H_{\text{spin}} = \sum_{i,j,k} c_{ijk} \sigma_i \otimes \sigma_j \otimes \sigma_k.$$

This expansion is always possible, since the set of n -fold tensor products of Pauli matrices constitutes a complete orthonormal basis for the linear vector space of all $2^n \times 2^n$ matrices. Because we have written the basis (4) in the form $|s_A\rangle |s_B\rangle |s_C\rangle$, these Pauli matrices can be associated with spin operators on each of the three quantum dots. For example, we can write $\sigma_1 \otimes \sigma_3 \otimes \sigma_0 = 2S_{A,x} \otimes 2S_{B,z} \otimes I \equiv 4S_{A,x} S_{B,z}$, where the notation $S_{W,i}$ means the Pauli operator σ_i applied to the electron in the quantum dot at W , and where I is the 2×2 identity matrix. (We exclude \hbar from the definition of the matrices σ_i ; thus, the c_{ijk} have the dimensions of energy.) In the case of an arbitrary 8×8 matrix, 64 complex numbers would be required to specify our c_{ijk} , but the operator (1) clearly has certain properties which constrain the values of the coefficients, such as Hermiticity, reflection symmetry, rotation symmetry, inversion symmetry, and invariance under permutation of the electrons' labels. Once these symmetries have been accounted for, the c_{ijk} may be characterized by just three real quantities:

$$H_{\text{spin}} = K_0 + K_2[AB](\mathbf{S}_A \cdot \mathbf{S}_B + \mathbf{S}_B \cdot \mathbf{S}_C) + K_2[AC]\mathbf{S}_A \cdot \mathbf{S}_C, \quad (6)$$

where $\mathbf{S}_W \cdot \mathbf{S}_V = S_{W,x} S_{V,x} + S_{W,y} S_{V,y} + S_{W,z} S_{V,z}$, and $K_2[ij]$ is the pairwise coupling coefficient between the spins of the electrons in dots i and j . Here and elsewhere, we use symmetry considerations to reduce the number of coupling coefficients in our equations; in this case, the reflection symmetry of Fig. 1 through the x - z plane implies that $K_2[AB] = K_2[BC]$. Physically, the constant $K_2[AB]$ quantifies the coupling between adjacent spins, while $K_2[AC]$ describes the coupling between the spins at opposite ends of the row.

Defining $\mathbf{S}_T = \mathbf{S}_A + \mathbf{S}_B + \mathbf{S}_C$, one finds that

$$\begin{aligned} (\mathbf{S}_A + \mathbf{S}_C)^2 &= \frac{3}{2} + 2\mathbf{S}_A \cdot \mathbf{S}_C \\ \mathbf{S}_T^2 &= \frac{9}{4} + 2(\mathbf{S}_A \cdot \mathbf{S}_B + \mathbf{S}_A \cdot \mathbf{S}_C + \mathbf{S}_B \cdot \mathbf{S}_C). \end{aligned}$$

Thus,

$$H_{\text{spin}} = L_0 + L_1 \mathbf{S}_T^2 + L'_1 (\mathbf{S}_A + \mathbf{S}_C)^2, \quad (7)$$

where

$$\begin{aligned} K_0 &= L_0 + \frac{9}{4}L_1 + \frac{3}{2}L'_1 \\ K_2[AB] &= 2L_1 \\ K_2[AC] &= 2L_1 + 2L'_1. \end{aligned} \quad (8)$$

The expansion (7) reveals that any simultaneous eigenstate of $(\mathbf{S}_A + \mathbf{S}_C)^2$ and \mathbf{S}_T^2 is also an eigenstate of H_{spin} . We can construct such simultaneous eigenstates by using the Clebsch-Gordan table twice, first to combine the spin of the electron in dot A with the spin of the electron in dot C , and then to combine that spin-1 (or spin-0) system with the spin of the electron in dot B :

$$\begin{aligned} |\frac{3}{2}, \frac{3}{2}; 1\rangle &= |\Psi(\uparrow\uparrow\uparrow)\rangle \\ |\frac{3}{2}, \frac{1}{2}; 1\rangle &= |\Psi(\uparrow\uparrow\downarrow)\rangle + |\Psi(\uparrow\downarrow\uparrow)\rangle + |\Psi(\downarrow\uparrow\uparrow)\rangle \\ |\frac{3}{2}, -\frac{1}{2}; 1\rangle &= |\Psi(\downarrow\downarrow\uparrow)\rangle + |\Psi(\downarrow\uparrow\downarrow)\rangle + |\Psi(\uparrow\downarrow\downarrow)\rangle \\ |\frac{3}{2}, -\frac{3}{2}; 1\rangle &= |\Psi(\downarrow\downarrow\downarrow)\rangle \\ |\frac{1}{2}, \frac{1}{2}; 1\rangle &= 2|\Psi(\uparrow\uparrow\downarrow)\rangle - |\Psi(\uparrow\uparrow\downarrow)\rangle - |\Psi(\downarrow\uparrow\uparrow)\rangle \\ |\frac{1}{2}, -\frac{1}{2}; 1\rangle &= 2|\Psi(\downarrow\downarrow\uparrow)\rangle - |\Psi(\downarrow\downarrow\uparrow)\rangle - |\Psi(\uparrow\downarrow\downarrow)\rangle \\ |\frac{1}{2}, \frac{1}{2}; 0\rangle &= |\Psi(\uparrow\uparrow\downarrow)\rangle - |\Psi(\downarrow\uparrow\uparrow)\rangle \\ |\frac{1}{2}, -\frac{1}{2}; 0\rangle &= |\Psi(\downarrow\downarrow\uparrow)\rangle - |\Psi(\uparrow\downarrow\downarrow)\rangle, \end{aligned} \quad (9)$$

where the indices on the left-hand side denote the values of S_T , $S_{T,z}$, and $|\mathbf{S}_A + \mathbf{S}_C|$ respectively. Although the states $|\Psi(s_A, s_B, s_C)\rangle$ are not orthonormal, the eight states (9) are orthogonal, and they are also eigenvectors of the 8×8 matrix (7), which means that H_{spin} has been diagonalized. To obtain the parameters $\{L_0, L_1, L'_1\}$, we will choose three eigenstates with different good quantum numbers, and observe that their energies can be evaluated either by matrix algebra or by integrating microscopically over the axes \mathbf{r}_i and the spins to compute the expectation value of (1):

$$\langle \Psi | H_{\text{spin}} | \Psi \rangle = \langle \Psi | H | \Psi \rangle. \quad (10)$$

Inserting (7) into the left-hand side, for three distinct combinations of the good quantum numbers $\{(\mathbf{S}_A + \mathbf{S}_C)^2, S_T^2\}$ yields

$$\begin{aligned} \frac{\langle \frac{3}{2}, \frac{3}{2}; 1 | H_{\text{spin}} | \frac{3}{2}, \frac{3}{2}; 1 \rangle}{\langle \frac{3}{2}, \frac{3}{2}; 1 | \frac{3}{2}, \frac{3}{2}; 1 \rangle} &= L_0 + \frac{15}{4}L_1 + 2L'_1 \\ \frac{\langle \frac{1}{2}, \frac{1}{2}; 1 | H_{\text{spin}} | \frac{1}{2}, \frac{1}{2}; 1 \rangle}{\langle \frac{1}{2}, \frac{1}{2}; 1 | \frac{1}{2}, \frac{1}{2}; 1 \rangle} &= L_0 + \frac{3}{4}L_1 + 2L'_1 \\ \frac{\langle \frac{1}{2}, \frac{1}{2}; 0 | H_{\text{spin}} | \frac{1}{2}, \frac{1}{2}; 0 \rangle}{\langle \frac{1}{2}, \frac{1}{2}; 0 | \frac{1}{2}, \frac{1}{2}; 0 \rangle} &= L_0 + \frac{3}{4}L_1 \end{aligned} \quad (11)$$

while the corresponding wave functions (9) turn the right-hand side into

$$\begin{aligned} E_{\frac{3}{2}, \frac{3}{2}; 1} &= \frac{\langle \Psi(\uparrow\uparrow\uparrow) | H | \Psi(\uparrow\uparrow\uparrow) \rangle}{\langle \Psi(\uparrow\uparrow\uparrow) | \Psi(\uparrow\uparrow\uparrow) \rangle} \\ E_{\frac{1}{2}, \frac{1}{2}; 1} &= \frac{\langle \Psi(\uparrow\uparrow\downarrow) | H | \Psi(\uparrow\uparrow\downarrow) \rangle + 2\langle \Psi(\uparrow\downarrow\uparrow) | H | \Psi(\uparrow\downarrow\uparrow) \rangle - 4\langle \Psi(\uparrow\uparrow\downarrow) | H | \Psi(\uparrow\downarrow\uparrow) \rangle + \langle \Psi(\uparrow\uparrow\downarrow) | H | \Psi(\downarrow\uparrow\uparrow) \rangle}{\langle \Psi(\uparrow\uparrow\downarrow) | \Psi(\uparrow\uparrow\downarrow) \rangle + 2\langle \Psi(\uparrow\downarrow\uparrow) | \Psi(\uparrow\downarrow\uparrow) \rangle - 4\langle \Psi(\uparrow\uparrow\downarrow) | \Psi(\uparrow\downarrow\uparrow) \rangle + \langle \Psi(\uparrow\uparrow\downarrow) | \Psi(\downarrow\uparrow\uparrow) \rangle} \\ E_{\frac{1}{2}, \frac{1}{2}; 0} &= \frac{\langle \Psi(\uparrow\uparrow\downarrow) | H | \Psi(\uparrow\uparrow\downarrow) \rangle - \langle \Psi(\uparrow\uparrow\downarrow) | H | \Psi(\downarrow\uparrow\uparrow) \rangle}{\langle \Psi(\uparrow\uparrow\downarrow) | \Psi(\uparrow\uparrow\downarrow) \rangle - \langle \Psi(\uparrow\uparrow\downarrow) | \Psi(\downarrow\uparrow\uparrow) \rangle} \end{aligned} \quad (12)$$

The inner products over the spin space are trivial:

$$\begin{aligned} \langle \Psi(\uparrow\uparrow\uparrow) | H | \Psi(\uparrow\uparrow\uparrow) \rangle &= 6H_I + 12H_\Delta - 12H_{AB} - 6H_{AC} \\ \langle \Psi(\uparrow\uparrow\downarrow) | H | \Psi(\uparrow\uparrow\downarrow) \rangle &= 6H_I - 6H_{AB} \\ \langle \Psi(\uparrow\downarrow\uparrow) | H | \Psi(\uparrow\downarrow\uparrow) \rangle &= 6H_I - 6H_{AC} \\ \langle \Psi(\uparrow\uparrow\downarrow) | H | \Psi(\uparrow\downarrow\uparrow) \rangle &= 6H_\Delta - 6H_{AB} \\ \langle \Psi(\uparrow\uparrow\downarrow) | H | \Psi(\downarrow\uparrow\uparrow) \rangle &= 6H_\Delta - 6H_{AC}, \end{aligned} \quad (13)$$

where

$$\begin{aligned} H_I &\equiv \langle ABC | H | ABC \rangle \\ H_{AB} &\equiv \langle ABC | H | BAC \rangle \\ H_{AC} &\equiv \langle ABC | H | CBA \rangle \\ H_\Delta &\equiv \langle ABC | H | CAB \rangle. \end{aligned} \quad (14)$$

(The subscripts here indicate the topology of each orbital exchange: I for idempotent, Δ for a cyclic permutation,

etc.) Similarly,

$$\begin{aligned}
\langle \Psi(\uparrow\uparrow\uparrow) | \Psi(\uparrow\uparrow\uparrow) \rangle &= 6 + 12\langle A|B \rangle^2 \langle A|C \rangle \\
&\quad - 12\langle A|B \rangle^2 - 6\langle A|C \rangle^2 \quad (15) \\
\langle \Psi(\uparrow\uparrow\downarrow) | \Psi(\uparrow\uparrow\downarrow) \rangle &= 6 - 6\langle A|B \rangle^2 \\
\langle \Psi(\uparrow\downarrow\uparrow) | \Psi(\uparrow\downarrow\uparrow) \rangle &= 6 - 6\langle A|C \rangle^2 \\
\langle \Psi(\uparrow\uparrow\downarrow) | \Psi(\uparrow\downarrow\uparrow) \rangle &= 6\langle A|B \rangle^2 \langle A|C \rangle - 6\langle A|B \rangle^2 \\
\langle \Psi(\uparrow\uparrow\downarrow) | \Psi(\downarrow\uparrow\uparrow) \rangle &= 6\langle A|B \rangle^2 \langle A|C \rangle - 6\langle A|C \rangle^2,
\end{aligned}$$

using the fact that the states (5) are normalized. Note that the symmetries of H and V have also been used, here and in (13), to reduce the number of terms in each expression. Using Eq. (2), the matrix products (14) and (15) may be evaluated by finding the one-body integrals

$$\begin{aligned}
\langle A|A \rangle &= 1 \quad (16) \\
\langle A|h|A \rangle &= \frac{\hbar\omega_o}{2048} [840x_b^{-2} + 7360x_b^{-1} + 7680] \\
\langle B|h|B \rangle &= \frac{\hbar\omega_o}{2048} [840x_b^{-2} + 640x_b^{-1} + 3072] \\
\langle A|B \rangle &= e^{-x_b} \\
\langle A|h|B \rangle &= \frac{\hbar\omega_o}{2048} [840x_b^{-2} + 2320x_b^{-1} + 2208 - 448x_b] e^{-x_b} \\
\langle A|C \rangle &= e^{-4x_b} \\
\langle A|h|C \rangle &= \frac{\hbar\omega_o}{2048} [840x_b^{-2} + 640x_b^{-1} + 3072 - 4096x_b] e^{-4x_b}
\end{aligned}$$

$$\begin{aligned}
\langle FG|w|UV \rangle &= \hbar\omega_o \left[\frac{2x_c\sqrt{x_b}}{|\mathbf{f} + \mathbf{u} - \mathbf{g} - \mathbf{v}|} e^{-(1/4)(|\mathbf{f}-\mathbf{u}|^2 + |\mathbf{g}-\mathbf{v}|^2)} \operatorname{erf} \left(\frac{|\mathbf{f} + \mathbf{u} - \mathbf{g} - \mathbf{v}|}{2\sqrt{2}} \right) \right], \quad |\mathbf{f} + \mathbf{u} - \mathbf{g} - \mathbf{v}| \neq 0; \quad (17) \\
\langle FG|w|UV \rangle &= \hbar\omega_o \left[\sqrt{\frac{2}{\pi}} x_c \sqrt{x_b} e^{-(1/4)(|\mathbf{f}-\mathbf{u}|^2 + |\mathbf{g}-\mathbf{v}|^2)} \right], \quad |\mathbf{f} + \mathbf{u} - \mathbf{g} - \mathbf{v}| = 0,
\end{aligned}$$

where the dimensionless parameter

$$x_b \equiv \frac{\frac{1}{2}m\omega_o^2 l^2}{\frac{1}{2}\hbar\omega_o} = \frac{m\omega_o l^2}{\hbar} \quad (18)$$

is the ratio of the height of the potential barrier between adjacent wells to the energy of the orbital ground state (5); the dimensionless parameter

$$x_c \equiv \frac{e^2}{\kappa l \hbar \omega_o} \quad (19)$$

is the ratio of the equilibrium Coulomb repulsion potential to the energy of the orbital ground state; $F, G, U, V \in \{A, B, C\}$; and $\mathbf{f} \equiv \sqrt{\frac{m\omega_o}{\hbar}} \mathbf{F}$, etc. (Note that our expression for $\langle FG|w|UV \rangle$ is a corrected version of Eqs. (28) and (29) in Ref. [32].) Combining Eqs. (8) and (11) - (17), we compute K_0 , $K_2[AB]$, and $K_2[AC]$.

and the Coulomb interaction term

Here and in the following section, we have estimated experimentally relevant values of x_b and x_c as is done in Ref. [1]. We assume that the width of the function (5), which is $2\sqrt{\hbar/m\omega_o}$, must be roughly equal to the separation between adjacent dots 2ℓ ; using (18), we conclude that $x_b \approx 1$. For GaAs heterostructure single dots, $\kappa \approx 13$, $m^* \approx 0.067 m_e$, and $\hbar\omega_o \approx 3$ meV, which according to (19) means that $x_c \approx 1.5$.

Fig. 3 shows the energy shift K_0 as a function of the system parameters $\{x_b, x_c\}$. As one might expect, this spin-independent quantity increases with increasing x_c and decreasing x_b (whenever ω_o decreases, there is greater orbital overlap and thus more Coulomb repulsion, irrespective of spin state). The coupling constants $K_2[AB]$ and $K_2[AC]$ are plotted in Fig. 4 and Fig. 5 respectively. We notice that they differ (which rules out the simple Heisenberg form $H_{\text{spin}} = J \sum_{i < j} (\mathbf{S}_i \cdot \mathbf{S}_j)$), and

that $K_2[AC]$ is only about an order of magnitude smaller than $K_2[AB]$. In the context of quantum computation, this demonstrates that a nearest-neighbor approximation for the coupling between dots is insufficient (see also Ref. [22], where a similar conclusion was reported using a low-energy Hubbard model with one electron per site).

FOUR-ELECTRON CASE USING A POLYNOMIAL POTENTIAL

For the case of four quantum dots arranged in a square of side $2l$, our formalism is more complex in detail but identical in structure. We outline the analysis here, and give details in the appendix.

The confining potential in the coordinate Hamiltonian

$$H = \sum_{i=1}^4 \left[\frac{\mathbf{p}_i^2}{2m} + V(\mathbf{r}_i) \right] + \sum_{i < j} \frac{e^2}{\kappa |\mathbf{r}_i - \mathbf{r}_j|} \quad (20)$$

now becomes

$$V(\mathbf{r}) = \frac{1}{2(2l)^6} m\omega_o^2 |\mathbf{r} - \mathbf{A}|^2 |\mathbf{r} - \mathbf{B}|^2 |\mathbf{r} - \mathbf{C}|^2 |\mathbf{r} - \mathbf{D}|^2 \quad (21)$$

(Fig. 6). The computational basis consists of 16 fully antisymmetrized vectors of the form

$$|\Psi(s_A, s_B, s_C, s_D)\rangle = \sum_P \delta_P P[|A\rangle |B\rangle |C\rangle |D\rangle \otimes |s_A\rangle |s_B\rangle |s_C\rangle |s_D\rangle]. \quad (22)$$

The form of $\phi(\mathbf{r})$ remains the same (Fig. 7).

Expanding H in terms of products of Pauli matrices,

$$H_{\text{spin}} = \sum_{i,j,k,l} c_{ijkl} \sigma_i \otimes \sigma_j \otimes \sigma_k \otimes \sigma_l,$$

we discover by applying the symmetries of (20) that four-body terms now appear with nonzero coupling coefficients:

$$\begin{aligned} H_{\text{spin}} = & K_0 + K_2[AB](\mathbf{S}_A \cdot \mathbf{S}_B + \mathbf{S}_B \cdot \mathbf{S}_C \\ & + \mathbf{S}_C \cdot \mathbf{S}_D + \mathbf{S}_D \cdot \mathbf{S}_A) \\ & + K_2[AC](\mathbf{S}_A \cdot \mathbf{S}_C + \mathbf{S}_B \cdot \mathbf{S}_D) \\ & + K_4[ABCD][(\mathbf{S}_A \cdot \mathbf{S}_B)(\mathbf{S}_C \cdot \mathbf{S}_D) \\ & + (\mathbf{S}_B \cdot \mathbf{S}_C)(\mathbf{S}_D \cdot \mathbf{S}_A)] \\ & + K_4[ACBD](\mathbf{S}_A \cdot \mathbf{S}_C)(\mathbf{S}_B \cdot \mathbf{S}_D), \end{aligned}$$

where $K_4[ijkl]$ is the four-body coupling coefficient among the spins of the electrons in dots i , j , k , and l . Physically, the constant $K_2[AB]$ describes the pairwise coupling between adjacent spins, while $K_2[AC]$ describes the pairwise coupling between non-adjacent spins, $K_4[ABCD]$ describes four-body interactions concentrating on pairs of adjacent spins, and $K_4[ACBD]$ describes four-body interactions concentrating on pairs of non-adjacent spins. We define $\mathbf{S}_T = \mathbf{S}_A + \mathbf{S}_B + \mathbf{S}_C + \mathbf{S}_D$; the operator identities

$$\begin{aligned} (\mathbf{S}_W + \mathbf{S}_V)^2 &= \frac{3}{2} + 2\mathbf{S}_W \cdot \mathbf{S}_V \\ \mathbf{S}_T^2 &= 3 + 2(\mathbf{S}_A \cdot \mathbf{S}_B + \mathbf{S}_B \cdot \mathbf{S}_C + \mathbf{S}_C \cdot \mathbf{S}_D + \mathbf{S}_D \cdot \mathbf{S}_A + \mathbf{S}_A \cdot \mathbf{S}_C + \mathbf{S}_B \cdot \mathbf{S}_D) \\ (\mathbf{S}_T^2)^2 &= \frac{27}{2} + 7(\mathbf{S}_A \cdot \mathbf{S}_B + \mathbf{S}_B \cdot \mathbf{S}_C + \mathbf{S}_C \cdot \mathbf{S}_D + \mathbf{S}_D \cdot \mathbf{S}_A + \mathbf{S}_A \cdot \mathbf{S}_C + \mathbf{S}_B \cdot \mathbf{S}_D) \\ &\quad + (\mathbf{S}_A \cdot \mathbf{S}_B)(\mathbf{S}_C \cdot \mathbf{S}_D) + (\mathbf{S}_B \cdot \mathbf{S}_C)(\mathbf{S}_D \cdot \mathbf{S}_A) + (\mathbf{S}_A \cdot \mathbf{S}_C)(\mathbf{S}_B \cdot \mathbf{S}_D) \end{aligned}$$

serve to transform H_{spin} into

$$\begin{aligned} H_{\text{spin}} = & L_0 + L_1 \mathbf{S}_T^2 + L'_1 [(\mathbf{S}_A + \mathbf{S}_C)^2 + (\mathbf{S}_B + \mathbf{S}_D)^2] \\ & + L_2 (\mathbf{S}_T^2)^2 + L'_2 (\mathbf{S}_A + \mathbf{S}_C)^2 (\mathbf{S}_B + \mathbf{S}_D)^2 \quad (23) \end{aligned}$$

where

$$\begin{aligned} K_0 &= L_0 + 3L_1 + 3L'_1 + \frac{45}{2}L_2 + \frac{9}{4}L'_2 \quad (24) \\ K_2[AB] &= 2L_1 + 24L_2 \\ K_2[AC] &= 2L_1 + 2L'_1 + 24L_2 + 3L'_2 \\ K_4[ABCD] &= 8L_2 \\ K_4[ACBD] &= 8L_2 + 4L'_2. \end{aligned}$$

Applying the Clebsch-Gordan table three times creates sixteen simultaneous eigenstates of $(\mathbf{S}_A + \mathbf{S}_C)^2$, $(\mathbf{S}_B + \mathbf{S}_D)^2$, and \mathbf{S}_T^2 . Inserting five of these states with different quantum numbers into (10) yields five equations for the five unknowns $\{L_0, L_1, L'_1, L_2, L'_2\}$ in terms of the eigenstate energies (see the appendix). As before, these energies may be expressed in closed form as functions of x_b and x_c by integrating the right-hand side of (10) explicitly.

The energy shift K_0 for the square case is plotted in Fig. 8; as before, this constant is largest for strongly Coulomb-coupled dots separated by low potential bar-

riers. Figs. 9, 10, 11, and 12 depict the coupling coefficients $K_2[AB]$, $K_2[AC]$, $K_4[ABCD]$, and $K_4[ACBD]$ respectively. The departure from the pairwise Heisenberg picture is even more pronounced here: we see that for physically relevant values of the parameters $\{x_b, x_c\}$, the four-body coefficient $K_4[ACBD]$ is of the same order of magnitude as the two-body coefficient $K_2[AC]$, while $K_4[ABCD]/K_2[AB] \sim 0.1$. Typically, $K_4[ACBD]$ is opposite in sign to $K_2[AC]$, leading to a particularly important competition between the two-body and four-body interactions.

GAUSSIAN POTENTIAL

While our model Hamiltonian improves on that of Ref. [17] by allowing the quantum dots to occupy a less symmetrical geometry, the potential (21) has certain other characteristics which are unlikely to describe an experimental arrangement; for example, it diverges at large

distances from the origin, and the single geometrical parameter x_b forces us to specify very narrow minima whenever we want a high barrier between them. We therefore repeat our analysis using a potential of the form

$$V(\mathbf{r}) = -V_0[e^{-\alpha|\mathbf{r}-\mathbf{A}|^2} + e^{-\alpha|\mathbf{r}-\mathbf{B}|^2} + e^{-\alpha|\mathbf{r}-\mathbf{C}|^2}] \quad (25)$$

(Fig. 13), which has two adjustable parameters. We will still use the localized orbital wave function (5) to form our computational basis states, with $\omega_o \equiv \sqrt{\frac{2V_0\alpha}{m}}$, since the first-order Taylor expansion of (25) is quadratic. Unless α is small compared to l^{-2} , however, this is a much coarser approximation than that of the previous sections, so we refine it by centering $\phi_A(\mathbf{r})$ and $\phi_C(\mathbf{r})$ at the points which minimize $\langle A|h|A \rangle$ and $\langle C|h|C \rangle$ (Fig. 14).

We proceed exactly as before, expanding both sides of (10) into overlap integrals and matrix elements of H ; the only necessary revisions are

$$\begin{aligned} \langle A|h|A \rangle &= \hbar\omega_o \left\{ \frac{3}{4} - \frac{x_v^{5/2} e^{-\frac{(p+2)^2 x_b}{x_v+1}} \left(1 + e^{\frac{8p x_b}{x_v+1}} + e^{\frac{(4p+4)x_b}{x_v+1}} - \operatorname{erf} \left[(px_v - 2) \sqrt{\frac{x_b}{x_v(x_v+1)}} \right] \right)}{2(x_v+1)^{3/2}} \right\} \\ \langle B|h|B \rangle &= \hbar\omega_o \left\{ \frac{3}{4} - \frac{x_v^{5/2} \left(1 + 2e^{-\frac{4x_b}{x_v+1}} \right)}{2(x_v+1)^{3/2}} \right\} \\ \langle A|B \rangle &= e^{-\frac{p^2 x_b}{4}} \\ \langle A|h|B \rangle &= \hbar\omega_o \left\{ \left(\frac{3}{4} - \frac{p^2 x_b}{8} \right) e^{-\frac{p^2 x_b}{4}} - \frac{x_v^{5/2} e^{-\frac{[p^2(x_v+2)+8p+16]x_b}{4(x_v+1)}} \left(1 + e^{\frac{4p x_b}{x_v+1}} + e^{\frac{(2p+4)x_b}{x_v+1}} \right)}{2(x_v+1)^{3/2}} \right\} \\ \langle A|C \rangle &= e^{-p^2 x_b} \\ \langle A|h|C \rangle &= \hbar\omega_o \left\{ \left(\frac{3}{4} - \frac{p^2 x_b}{2} \right) e^{-p^2 x_b} - \frac{x_v^{5/2} e^{\frac{[2p^2(x_v+1)+4]x_b}{x_v+1}} \left(2e^{p^2 x_b} + e^{\frac{x_b[p^2(x_v+1)+4]}{x_v+1}} \right)}{2(x_v+1)^{3/2}} \right\}, \end{aligned}$$

where the new dimensionless quantity

$$x_v \equiv \frac{2V_0}{\hbar\omega_o} \quad (26)$$

is the ratio of the individual well depth V_0 to the ground state harmonic oscillator energy, and the localized orbital wave functions near \mathbf{A} and \mathbf{C} are centered at $x = \mp pl$ ($p = 2$ would mean that their locations are unchanged from the quadratic case, for example).

A potential of the form (25) is most suitable for quantum computation when $\alpha\ell^2$ is close to 1; if the inverted

Gaussian decays too quickly in space, the spin coupling in the system becomes negligible, and if it decays too slowly, the local minima in V tend to coalesce at the center. Using $\frac{1}{2}\hbar\omega_o \sim 1$ meV, $V_0 \approx 3$ meV [1], and our prior estimate of $x_c \approx 1.5$, we obtain the relation $x_b \approx x_v \sim 3$, by applying (18), (19), and (26).

Figs. 15 through 17 show the resulting dependence of the coupling constants K_0 , $K_2[AB]$, and $K_2[AC]$ on the parameters x_b and x_v . Noting that the parameter x_c had very little effect on the final results of the previous sec-

tions (and in any event depends on quantities, such as κ , which are difficult to tune experimentally), we henceforth set $x_c = 1.5$. The absolute sizes of all three coupling coefficients are smaller for the potential (25) than they were for (3). For the constant term K_0 , this is not surprising, since the total energy of a given orbital state now has an upper bound of zero rather than a lower bound of $\frac{3}{2}\hbar\omega_o$: its kinetic and potential energies are now opposite in sign. $K_2[AB]$ and $K_2[AC]$ have decreased because the parameters x_b and x_v , in the ranges defined above, separate the localized orbitals more completely than does the single parameter x_b in the polynomial case. The spin coupling is still largest for broad dots (that is, when $\alpha\ell^2$ is small), and the ratio $K_2[AC]/K_2[AB]$ has remained appreciable ($\sim 5\%$), as we have confirmed by studying $K_2[AB](x_b, x_v)$ and $K_2[AC](x_b, x_v)$ on a logarithmic scale.

In the $N = 4$ case, wherein

$$V(\mathbf{r}) = -V_0 \left[e^{-\alpha|\mathbf{r}-\mathbf{A}|^2} + e^{-\alpha|\mathbf{r}-\mathbf{B}|^2} + e^{-\alpha|\mathbf{r}-\mathbf{C}|^2} + e^{-\alpha|\mathbf{r}-\mathbf{D}|^2} \right]$$

(Figs. 18 and 19), we again see that most of the intermediate steps in our calculation are independent of V , and make the required changes to our one-body integrals (see Appendix). Figs. 20 through 24 show the coefficients K_0 , $K_2[AB]$, $K_2[AC]$, $K_4[ABCD]$, and $K_4[ACBD]$, respectively. As in the quadratic case, the four-body coupling is about a quarter the size of the two-body coupling for adjacent dots, and of the same order of magnitude (and opposite in sign) for non-adjacent dots, as is confirmed by plotting $K_2[AB](x_b, x_v)$, $K_2[AC](x_b, x_v)$, $K_4[ABCD](x_b, x_v)$, and $K_4[ACBD](x_b, x_v)$ on a logarithmic scale.

COMPUTING IN THE PRESENCE OF FOUR-BODY INTERACTIONS USING ENCODED QUBITS

We have shown that coupling three dots simultaneously quantitatively modifies the value of the exchange constant, and that coupling four dots simultaneously switches on a four-body interaction term of the form $K_4[ABCD](\mathbf{S}_A \cdot \mathbf{S}_B)(\mathbf{S}_C \cdot \mathbf{S}_D)$ and its permutations. This conclusion appears to be robust under changes in dot geometry and in the confining potential. A natural question is whether there exist methods to cancel the four-body correction. The issue is particularly urgent when one considers encoded quantum computation (EQC). In many known constructions of universal gates for EQC [5, 6, 7, 8, 9, 10, 23, 24, 25, 26, 27, 28, 30], there arises the need to simultaneously couple several spins. One of the most popular codes, described in detail below, uses four spins per encoded, or logical qubit [5, 6, 8, 9, 10, 23, 24, 25, 26, 27, 28]. For this code, universal computation requires that four spins be coupled

at the same time using pairwise Heisenberg interactions. Hence a priori it appears that EQC using the four-qubit code suffers from a fundamental flaw. We now explore whether the four-qubit code may be implemented in such a way that each four-body coupling is either cancelled or reduced to an overall phase. Our findings highlight problems that the four-body terms present in the context of EQC, and also provide an interesting perspective on how the four-body terms may need to be dealt with in general.

The Code

Let us describe the four-spin DFS code, first proposed in Ref. [26] in the context of providing immunity against collective decoherence processes (see Ref. [28] for a review). Let the singlet and triplet states of two electrons i, j be denoted as

$$\begin{aligned} |s\rangle_{ij} &\equiv |S = 0, m_S = 0\rangle = \frac{1}{\sqrt{2}} (|\Psi(\uparrow\downarrow)\rangle - |\Psi(\downarrow\uparrow)\rangle) \\ |t_-\rangle_{ij} &\equiv |S = 1, m_S = -1\rangle = |\Psi(\downarrow\downarrow)\rangle \\ |t_0\rangle_{ij} &\equiv |S = 1, m_S = 0\rangle = \frac{1}{\sqrt{2}} (|\Psi(\uparrow\downarrow)\rangle + |\Psi(\downarrow\uparrow)\rangle) \\ |t_+\rangle_{ij} &\equiv |S = 1, m_S = 1\rangle = |\Psi(\uparrow\uparrow)\rangle. \end{aligned}$$

Then a single encoded DFS qubit is formed by the two singlets of four spins, i.e., the two states with zero total spin $S_T = |\mathbf{S}_A + \mathbf{S}_B + \mathbf{S}_C + \mathbf{S}_D|$. These states are formed by combining two singlets of two pairs of spins ($|0_L\rangle$), or triplets of two pairs of spins, with appropriate Clebsch-Gordan coefficients ($|1_L\rangle$):

$$\begin{aligned} |0_L\rangle &= |s\rangle_{AB} \otimes |s\rangle_{CD} \\ &= \frac{1}{2} (|\Psi(\uparrow\downarrow\uparrow\downarrow)\rangle + |\Psi(\downarrow\uparrow\downarrow\uparrow)\rangle \\ &\quad - |\Psi(\uparrow\downarrow\downarrow\uparrow)\rangle - |\Psi(\downarrow\uparrow\uparrow\downarrow)\rangle) \end{aligned} \quad (27)$$

$$- |\Psi(\uparrow\downarrow\downarrow\uparrow)\rangle - |\Psi(\downarrow\uparrow\uparrow\downarrow)\rangle) \quad (28)$$

$$\begin{aligned} |1_L\rangle &= \frac{1}{\sqrt{3}} (|t_-\rangle_{AB} \otimes |t_+\rangle_{CD} - |t_0\rangle_{AB} \otimes |t_0\rangle_{CD} \\ &\quad + |t_+\rangle_{AB} \otimes |t_-\rangle_{CD}) \\ &= \frac{1}{\sqrt{3}} (2|\Psi(\uparrow\uparrow\downarrow\downarrow)\rangle + 2|\Psi(\downarrow\downarrow\uparrow\uparrow)\rangle - |\Psi(\uparrow\downarrow\uparrow\downarrow)\rangle \\ &\quad - |\Psi(\downarrow\uparrow\downarrow\uparrow)\rangle - |\Psi(\uparrow\downarrow\downarrow\uparrow)\rangle - |\Psi(\downarrow\uparrow\uparrow\downarrow)\rangle). \end{aligned} \quad (29)$$

As shown in Refs. [5, 6], the Heisenberg interaction $\mathbf{S}_i \cdot \mathbf{S}_j$ can be used all by itself to implement universal quantum computation on this type of code. The Heisenberg interaction is closely related to the exchange operator E_{ij} , defined as

$$E_{ij} = \begin{pmatrix} 1 & & & \\ & 0 & 1 & \\ & 1 & 0 & \\ & & & 1 \end{pmatrix} \quad (30)$$

via $E_{ij} = \frac{1}{2}(4\mathbf{S}_i \cdot \mathbf{S}_j + I)$. The difference in their action as gates is only a phase, so that we will use E_{ij} and

$\mathbf{S}_i \cdot \mathbf{S}_j$ interchangeably from now on, and denote $E_{ij} \simeq \mathbf{S}_i \cdot \mathbf{S}_j$. The E_{ij} have a simple action on the electronic spin up/down states, as seen from the matrix representation (30): the states $|00\rangle$ and $|11\rangle$ are invariant, whereas $|01\rangle$ and $|10\rangle$ are exchanged. Using this, it is simple to show that, in the $\{|0_L\rangle, |1_L\rangle\}$ basis, the exchange operators can be written as [6, 27]

$$\begin{aligned} E_{AB} &= E_{CD} = \begin{pmatrix} -1 & 0 \\ 0 & 1 \end{pmatrix} = -\bar{Z} \\ E_{AC} &= E_{BD} = \frac{\sqrt{3}}{2}\bar{X} + \frac{1}{2}\bar{Z} \\ E_{AD} &= E_{BC} = -\frac{\sqrt{3}}{2}\bar{X} + \frac{1}{2}\bar{Z}, \end{aligned} \quad (31)$$

where \bar{X}, \bar{Z} are the encoded Pauli matrices σ_x, σ_z , i.e., the Pauli matrices acting on the $|0_L\rangle, |1_L\rangle$ states. It follows from the Euler angle formula, $e^{-i\omega\mathbf{n}\cdot\boldsymbol{\sigma}} = e^{-i\beta\sigma_z}e^{-i\theta\sigma_x}e^{-i\alpha\sigma_z}$ (a rotation by angle ω about the axis \mathbf{n} , given in terms of three successive rotations about the z and x axes), that one can perform all single encoded-qubit operations on the DFS states, simply by switching the exchange interaction on and off. Note that the Euler angle formula is satisfied by any pair of non-parallel axes, but orthogonal axes may be more convenient. One can obtain an encoded σ_x operation by switching on two interactions simultaneously for the appropriate time intervals:

$$\bar{X} = -2 \left(E_{AC} + \frac{1}{2}E_{AB} \right) / \sqrt{3} = (E_{AC} - E_{AD}) / \sqrt{3}.$$

Use of the Euler angle formula requires a Hamiltonian which is a sum of exchange terms with controllable coefficients $J_{ij}(t)$:

$$H_S = \sum_{i \neq j} J_{ij}(t) E_{ij}.$$

This is achievable, e.g., by using local magnetic fields [1, 19, 20, 33, 34], by ferroelectric gates [35], or by optical rectification [36]. It is important to emphasize that the last two methods [35, 36] do not require magnetic field control, hence overcome at least in part the problems with EQC raised in Refs. [21, 22]. This is an important advantage with regards to EQC, which renders these electrical-only type control methods distinctly preferable to those using magnetic fields. However, residual magnetic fields, e.g., due to nuclear spin impurities, do remain a problem, especially in the group III-V semiconductors, such as GaAs [37]. In silicon-based architectures this problem can be minimized by isotopic purification [38].

Effect of the Four-Body Terms on a Single Encoded Qubit

Let us now consider how the four-body terms act on the DFS code. Using the results above, we find that

$$(\mathbf{S}_A \cdot \mathbf{S}_B)(\mathbf{S}_C \cdot \mathbf{S}_D) \simeq E_{AB}E_{CD} = (-\bar{Z})^2 = I,$$

where I is the identity operator. Also,

$$\begin{aligned} E_{AC}E_{BD} &= \left(\frac{\sqrt{3}}{2}\bar{X} + \frac{1}{2}\bar{Z} \right)^2 \\ &= \frac{1}{4} \left(3I + I + \sqrt{3}(\bar{X}\bar{Z} + \bar{Z}\bar{X}) \right) = I, \end{aligned}$$

and similarly $E_{AD}E_{BC} = I$. Thus all fourth-order terms $(\mathbf{S}_i \cdot \mathbf{S}_j)(\mathbf{S}_k \cdot \mathbf{S}_l) \propto I$ as long we restrict their action to the subspace encoding one qubit. This implies that the encoding into the 4-qubit DFS is immune to the fourth-order terms. In other words, when this encoding is used, the problem of the computational errors induced by the undesired fourth-order terms simply disappears, as long as we restrict our attention to a single encoded qubit.

Two Encoded Qubits

We must also be able to couple encoded qubits via a non-trivial gate such as controlled-phase: $CP = \text{diag}(-1, 1, 1, 1)$. This is one way to satisfy the requirements for universal quantum computation [39], though it is also possible to complete the set of single-qubit gates by measurements [40]. Two encoded qubits of the form (28), (29) occupy a four-dimensional subspace of the zero total spin subspace of 8 spins. This subspace is 14-dimensional. A very useful graphical way of seeing this, introduced in Ref. [6] but also known as a Bratteli diagram, is depicted in Fig. 25.

As more spins are added (horizontal axis), there are more possibilities for constructing a state with given total spin (vertical axis). In the case of four spins there are two paths leading from the origin to $S_T = 0$; these correspond exactly to the $|0_L\rangle$ and $|1_L\rangle$ code states. For eight spins there are 14 such paths. Only four of these correspond to the four basis states $|0_L0_L\rangle, |0_L1_L\rangle, |1_L0_L\rangle, |1_L1_L\rangle$. It is convenient to label paths according to the intermediate total spin: the state $|S_1, S_2, S_3, S_4, S_5, S_6, S_7, S_8\rangle$, where S_k is the total spin of k spin-1/2 particles, uniquely corresponds to a path in Fig. 25 (we omit the origin in this notation), and the S_k form a complete set of commuting observables [6]. E.g.,

$$\begin{aligned}
|0_L 0_L\rangle &= |1/2, 0, 1/2, 0, 1/2, 0, 1/2, 0\rangle = \nearrow \searrow \nearrow \searrow \nearrow \searrow \nearrow \searrow \\
|0_L 1_L\rangle &= |1/2, 0, 1/2, 0, 1/2, 1, 1/2, 0\rangle = \nearrow \searrow \nearrow \searrow \nearrow \searrow \nearrow \searrow \\
|1_L 0_L\rangle &= |1/2, 1, 1/2, 0, 1/2, 0, 1/2, 0\rangle = \nearrow \searrow \nearrow \searrow \nearrow \searrow \nearrow \searrow \\
|1_L 1_L\rangle &= |1/2, 1, 1/2, 0, 1/2, 1, 1/2, 0\rangle = \nearrow \searrow \nearrow \searrow \nearrow \searrow \nearrow \searrow .
\end{aligned}$$

On the right we have indicated the path in Fig. 25 corresponding to each state. The other 10 states with zero total spin can be similarly described. Thus the set of 14 states $\{|S_1, S_2, S_3, S_4, S_5, S_6, S_7, 0\rangle\}$ forms a basis for the subspace of zero total spin of 8 spin-1/2 particles. Henceforth we will find it convenient to represent exchange operators in this basis. We will order the 14 basis states as follows: first the four code states $|0_L 0_L\rangle, |0_L 1_L\rangle, |1_L 0_L\rangle, |1_L 1_L\rangle$ as above, then

$$\begin{aligned}
&|1/2, 0, 1/2, 1, 1/2, 0, 1/2, 0\rangle, |1/2, 1, 1/2, 1, 1/2, 0, 1/2, 0\rangle, \\
&|1/2, 0, 1/2, 1, 1/2, 1, 1/2, 0\rangle, |1/2, 1, 1/2, 1, 1/2, 1, 1/2, 0\rangle, \\
&|1/2, 0, 1/2, 1, 3/2, 1, 1/2, 0\rangle, |1/2, 1, 3/2, 1, 1/2, 0, 1/2, 0\rangle, \\
&|1/2, 1, 3/2, 1, 3/2, 1, 1/2, 0\rangle, |1/2, 1, 3/2, 2, 3/2, 1, 1/2, 0\rangle, \\
&|1/2, 1, 1/2, 1, 3/2, 1, 1/2, 0\rangle, |1/2, 1, 3/2, 1, 1/2, 1, 1/2, 0\rangle.
\end{aligned}$$

E.g., in this basis the operator E_{DE} has the representation[41]

$$E_{DE} = \begin{pmatrix} \frac{1}{2} & & & & & & & & & & & & & & & & & & \\ & \frac{1}{2} & & & & & & & & & & & & & & & & & \\ & & \frac{1}{2} & & & & & & & & & & & & & & & & \\ & & & \frac{1}{2} & & & & & & & & & & & & & & & \\ \frac{\sqrt{3}}{2} & & & & & & & & & & & & & & & & & & \\ & \frac{\sqrt{3}}{2} & & & & & & & & & & & & & & & & & \\ & & \frac{\sqrt{3}}{2} & & & & & & & & & & & & & & & & \\ & & & \frac{\sqrt{3}}{2} & & & & & & & & & & & & & & & \\ & & & & -\frac{1}{2} & & & & & & & & & & & & & & \\ & & & & & -\frac{1}{2} & & & & & & & & & & & & & \\ & & & & & & -\frac{1}{2} & & & & & & & & & & & & \\ & & & & & & & -\frac{1}{2} & & & & & & & & & & & \\ & & & & & & & & 1 & & & & & & & & & & \\ & & & & & & & & & 1 & & & & & & & & & \\ & & & & & & & & & & \frac{1}{4} & \frac{\sqrt{15}}{4} & & & & & & & \\ & & & & & & & & & & \frac{\sqrt{15}}{4} & -\frac{1}{4} & & & & & & & \\ & & & & & & & & & & & & 1 & & & & & & \\ & & & & & & & & & & & & & 1 & & & & & \end{pmatrix}$$

Recall that the first four rows refer to the code space. It is then clear that E_{DE} mixes the code space with four of the remaining ten states that have zero total spin. This is a general feature of all exchange operators acting on two code blocks simultaneously. For this reason it is

impossible to couple two code blocks in one step, while preserving the code space.

Enacting an Encoded Controlled-Phase Gate

For the 4-qubit code above, procedures implementing a CP gate were first given in Refs. [5, 6]. Recently, Bacon [29, App. E] found a simplified scheme which is a useful starting point for our purposes. Bacon's implementation of a CP gate between two pairs of 4-qubit blocks (qubits A - D and qubits E - H) involves a sequence of 14 elementary gates, each of which requires that several simultaneous exchange interactions be switched on and off. We will here take the approach of utilizing Bacon's construction, while making some modifications due to the appearance of three- and four-body corrections. For ease of visualization, we will assume that the two blocks are squares of side $2l$ and that dots D and E are separated by a distance $2l$, although nearly all of the following calculations are independent of the exact spatial relationship between the blocks.

The gates are (adapting the notation of [29, App. E])

$$\begin{aligned} U_1 &= \exp \left[\frac{i\pi}{\sqrt{3}} \left(E_{DE} + \frac{1}{2} \sum_{A=i<j}^D E_{ij} \right) \right] \\ U_2 &= \exp \left[\frac{i\pi}{4\sqrt{2}} \left(-3E_{EF} - \frac{2}{3} (E_{FG} + E_{FH} + E_{GH}) \right) \right] \\ U_3 &= \exp \left[\frac{i\pi}{4\sqrt{2}} \left(-3E_{CD} - \frac{2}{3} (E_{AB} + E_{AC} + E_{BC}) \right) \right] \\ U_5 &= \exp \left[\frac{i\pi}{\sqrt{3}} \left(E_{FG} + \frac{1}{2} E_{GH} \right) \right] \\ U_6 &= \left(U_A U_B U_A^\dagger U_B^\dagger \right)^2, \end{aligned}$$

where

$$\begin{aligned} U_A &= \exp \left[-\frac{i}{2} \cos^{-1}(-1/3) E_{DE} \right] \\ U_B &= \exp \left[-\frac{i\pi}{2} \sum_{A=i<j}^D E_{ij} \right]. \end{aligned}$$

In terms of these gates, the controlled-phase gate can be

written as

$$CP = U_1^\dagger (U_2^\dagger U_3^\dagger) U_5^\dagger U_6 U_5 (U_3 U_2) U_1,$$

where $U_3 U_2$ can be executed in one step since by inspection the two gates operate on the two blocks separately (and identically). This gate sequence operates in the entire 14-dimensional subspace of $S_T = 0$ states of 8 spins: the code space is left after application of U_1 , but is returned to at the end of the sequence, when U_1^\dagger is applied. Hence our single-qubit considerations above do not apply: even if a four-body interaction acts as the identity operator on a single encoded qubit, it may act non-trivially in the larger $S_T = 0$ space. We must therefore carefully analyze the action of this gate sequence in light of the three- and four-body corrections.

The key point in Bacon's construction of the gate sequence is to ensure that each gate acts "classically," i.e., it only couples a given $S_T = 0$ basis state to another, without creating superpositions of such basis states (that the gates above act in this manner is not at all simple to see directly, but is the reason for the particular choice of angles in the gates). Here we will show that, in order to still satisfy this key point, it is necessary to tune the four-body exchange coupling constants. Thus, to enact a CP gate in the presence of four-body interactions, there needs to be sufficient flexibility in tuning the four-body coupling. We note that there are other ways to obtain a CP gate [30]; our point here is mostly to explore the implications of the four-body terms in a context of some general interest. Let us now consider each of the gates in detail, in increasing order of complexity.

The U_A Gate

U_A only involves a single exchange interaction, and so is unmodified in the presence of the three- and four-body corrections:

three-body correction to the exchange constants. In addition, a coupling between dot F and dot H will arise, which forces our modified U_5 gate to have the form

U_5 involves dots F , G , and H , with dots F and H simultaneously coupled to G , and hence experiences a

$$U'_5 = \exp\left[\frac{i\pi}{\sqrt{3}}\left(E_{FG} + \frac{1}{2}E_{GH} + J'_5 E_{FH}\right)\right]$$

$$= \begin{pmatrix} p & \Phi \\ \Phi & p^* \\ & p & \Phi \\ & \Phi & p^* \\ & & p & \Phi \\ & & \Phi & p \\ & & & p^* \\ & & & e^{\frac{i\pi(2J_5+3)}{2\sqrt{3}}} \\ & & & & p \\ & & & & e^{\frac{i\pi(2J_5+3)}{2\sqrt{3}}} \\ & & & & & e^{\frac{i\pi(2J_5+3)}{2\sqrt{3}}} \\ & & & & & & e^{\frac{i\pi(2J_5+3)}{2\sqrt{3}}} \\ & & & & & & & \Phi \\ & & & & & & & & p^* \end{pmatrix},$$

It is seen that this gate operates “classically,” and is non-diagonal, only when J'_5 is either 0 or chosen such that Λ

$$\begin{aligned}\Lambda &= \sqrt{\frac{4}{3}(J'_5)^2 - 2J'_5 + 1} \\ p &= \cos\left[\frac{\pi}{2}\right] \Lambda + \frac{iJ'_5}{\sqrt{3}\Lambda} \sin\left[\frac{\pi}{2}\Lambda\right] \\ \Phi &= \frac{i}{J'}(1 - J'_5) \sin\left[\frac{\pi}{2}\Lambda\right]\end{aligned}$$

is an even integer. In both cases, we recover Bacon's functional form:

$$U_5 = \begin{pmatrix} i & & & & & & & & \\ & i & & & & & & & \\ & & i & & & & & & \\ & & & i & & & & & \\ & & & & i & & & & \\ & & & & & i & & & \\ & & & & & & e^{i\frac{\sqrt{3}\pi}{2}} & & \\ & & & & & & & e^{i\frac{\sqrt{3}\pi}{2}} & \\ & & & & & & & & e^{i\frac{\sqrt{3}\pi}{2}} & \\ & & & & & & & & & i \end{pmatrix}.$$

The U_B Gate

Bacon's U_B gate is

$$\begin{aligned} U_B &= \exp \left[-\frac{i\pi}{2} \left(\sum_{A=i < j}^D E_{ij} \right) \right] \\ &= \text{diag}(1, 1, 1, 1, -1, -1, -1, \\ &\quad -1, -1, -1, -1, -1, -1, -1). \end{aligned}$$

U_B involves coupling between four dots, so experiences both quantitative three-body corrections and a four-body qualitative correction. Since the four spins in U_B are coupled symmetrically, the form of the four-body correction must also be symmetric:

$$\begin{aligned} U'_B &= \exp \left[-\frac{i\pi}{2} \left(\sum_{A=i < j}^D E_{ij} + J'_B (E_{AB}E_{CD} \right. \right. \\ &\quad \left. \left. + E_{AC}E_{BD} + E_{AD}E_{BC}) \right) \right] \\ &= \text{diag}(\gamma^{-3}, \gamma^{-3}, \gamma^{-3}, \gamma^{-3}, -\gamma, -\gamma, -\gamma, \\ &\quad -\gamma, -\gamma, -\gamma, -\gamma, -\gamma^{-3}, -\gamma, -\gamma), \end{aligned}$$

where $\gamma = e^{\frac{i\pi}{2}J'_B}$. Note that because U'_B forms part of the U'_6 gate, that acts on $S_T = 0$ states outside of the code space, the action of the four-body terms in it is nontrivial for arbitrary J'_B . However, upon setting J'_B to any integer value we recover U_B , up to an overall phase.

The U_2, U_3 Gates

U_2, U_3 similarly involve coupling between four dots inside a fixed code block, so also experience both quantitative three-body corrections and a four-body qualitative correction. In this case the Heisenberg couplings are not symmetric, so we do not assume that the four-body terms

are all turned on with equal coupling constants:

$$\begin{aligned} U'_2 &= \exp \left[\frac{i\pi}{4\sqrt{2}} \left(-3E_{EF} - \frac{2}{3}(E_{FG} + E_{FH} + E_{GH}) \right. \right. \\ &\quad \left. \left. + J'_2 E_{EF}E_{GH} + J''_2 (E_{AC}E_{BD} + E_{EH}E_{FG}) \right) \right] \\ &= \begin{pmatrix} \delta & & & & & & & & \\ & \epsilon & & & & & & & \\ & & \delta & & & & & & \\ & & & \epsilon & & & & & \\ & & & & \zeta & & & & \\ & & & & & \zeta & & & \\ & & & & & & \eta & & \rho \\ & & & & & & & \eta & \rho \\ & & & & & & \rho & \eta^* & \\ & & & & & & & \zeta & \eta^* \\ & & & & & & & & e^{i\pi \frac{(-5+J'_2+2J''_2)}{4\sqrt{2}}} & \rho \\ & & & & & & & & & \rho \\ & & & & & & & & & \eta^* \end{pmatrix}, \end{aligned}$$

and

$$\begin{aligned} U'_3 &= \exp \left[\frac{i\pi}{4\sqrt{2}} \left(-3E_{CD} - \frac{2}{3}(E_{AB} + E_{AC} + E_{BC}) \right. \right. \\ &\quad \left. \left. + J'_3 E_{AB}E_{CD} + J''_3 (E_{AC}E_{BD} + E_{AD}E_{BC}) \right) \right] \\ &= \begin{pmatrix} \delta & & & & & & & & \\ & \delta & & & & & & & \\ & & \epsilon & & & & & & \\ & & & \epsilon & & & & & \\ & & & & \zeta & & & & \\ & & & & & \eta & & & \rho \\ & & & & & & \zeta & & \\ & & & & & & & \eta & \rho \\ & & & & & & \rho & \eta^* & \\ & & & & & & & \eta^* & \rho \\ & & & & & & & & e^{i\pi \frac{(-5+J'_3+2J''_3)}{4\sqrt{2}}} & \rho \\ & & & & & & & & & \eta \\ & & & & & & & & & \eta^* \end{pmatrix}, \end{aligned}$$

where

$$\begin{aligned} \nu &= \sqrt{3(J'_k)^2 + 3(J''_k)^2 - 6J'_kJ''_k - 16J'_k + 16J''_k + 24} \\ \delta &= e^{i\pi \frac{1}{4\sqrt{2}}(J'_k + 2J''_k + 3)} \\ \epsilon &= e^{i\pi \frac{1}{4\sqrt{2}}(J'_k + 2J''_k + 3)} \\ \zeta &= e^{-i\pi \frac{1}{4\sqrt{2}}(J'_k + 3)} \\ \eta &= e^{-i\pi \frac{1}{4\sqrt{2}}} \left[\cos \left(\frac{\pi\nu}{4\sqrt{6}} \right) - \frac{1}{\sqrt{3}\nu} (J'_k - J''_k) \sin \left(\frac{\pi\nu}{4\sqrt{6}} \right) \right] \\ \rho &= \frac{\sqrt{2}(3 - J'_k + J''_k)}{\sqrt{3}\nu} e^{-\frac{i\pi}{4\sqrt{2}}[1+J''_k-\frac{\nu}{\sqrt{3}}]} \left[1 - e^{\frac{i\pi\nu}{2\sqrt{6}}} \right], \end{aligned}$$

and $k = 2$ (3) for U'_2 (U'_3). It turns out that these two gates can act “classically” only when $\eta = 0$, which leads to a transcendental equation relating J'_k and J''_k ($J'_k = J''_k$ is one set of solutions).

The U_1 Gate

The U_1 gate is qualitatively different from all the previous gates. It involves an interaction between five dots

$$\begin{aligned}
x &= \left(9(1 + 4J'_b - 4J'_d) + 48 \left(J'^2_a + J'^2_b - J'_b J'_d + J'^2_d - J'_a (J'_b + J'_d) \right) \right)^{1/2} \\
y &= \left(3 + 8J'^2_a + 8J'^2_b + 9J'_c - J'_b (9 + 6J'_c - 4J'_d) + 2(3J'_c - 2J'_d)^2 \right. \\
&\quad \left. - 2J'_a (-3 + 7J'_b + 3J'_c - 2J'_d) - 6J'^2_d \right)^{1/2} \\
\chi_{\pm} &= \left(\cos(\pi x/6) \pm 2i\sqrt{3} \frac{(2J'_a - J'_b - J'_d)}{x} \sin(\pi x/6) \right) e^{i\pi \frac{\sqrt{3}}{6} (1+2J'_a+2J'_b+2J'_d)} \\
\lambda &= \frac{3i(1 + 2J'_b - 2J'_d)}{x} \sin(\pi x/6) e^{i\pi \frac{\sqrt{3}}{6} (1+2J'_a+2J'_b+2J'_d)} \\
\xi &= e^{i\pi \frac{1}{\sqrt{3}} (2-J'_a-J'_b+2J'_d)} \\
\theta &= \xi e^{i\pi \sqrt{3} J'_c} \\
\tau_{\pm} &= \left(\cos\left(\frac{\pi y}{\sqrt{6}}\right) \pm \frac{i(3 + 8J'_a - 7J'_b - 3J'_c + 2J'_d)}{2\sqrt{2}y} \sin\left(\frac{\pi y}{\sqrt{6}}\right) \right) e^{i\pi \frac{1}{\sqrt{3}} (2+J'_a+J'_b-2J'_d)} \\
\mu &= \frac{\sqrt{15}(J'_b - 3J'_c + 2J'_d - 1)}{2\sqrt{2}iy} \sin\left(\frac{\pi y}{\sqrt{6}}\right) e^{i\pi \frac{1}{\sqrt{3}} (2+J'_a+J'_b-2J'_d)}.
\end{aligned} \tag{33}$$

In comparison, Bacon's U_1 gate has the form

$$U_1 = \begin{pmatrix} & & & \Omega & & & & & & & \\ & & & & \Omega & & & & & & \\ & & & & & \Omega & & & & & \\ \Omega & & & & & & \Omega & & & & \\ & \Omega & & & & & & & & & \\ & & \Omega & & & & & & & & \\ & & & \Omega & & & & & & & \\ & & & & \Xi & & & & & & \\ & & & & & \Xi & & & & & \\ & & & & & & \Gamma & \Delta & & & \\ & & & & & & \Delta & \Theta & & & \\ & & & & & & & & \Xi & & \\ & & & & & & & & & \Xi & \end{pmatrix}, \tag{34}$$

where

$$\begin{aligned}
\Omega &= ie^{i\frac{\pi}{2\sqrt{3}}} \\
\Xi &= e^{i\frac{2\pi}{\sqrt{3}}} \\
\Delta &= \frac{i}{2}\sqrt{\frac{5}{2}}e^{i\frac{2\pi}{\sqrt{3}}}\sin\left(\frac{\pi}{\sqrt{2}}\right) \\
\Theta &= e^{i\frac{2\pi}{\sqrt{3}}}\left(\cos\left(\frac{\pi}{\sqrt{2}}\right) + i\sqrt{\frac{3}{8}}\sin\left(\frac{\pi}{\sqrt{2}}\right)\right) \\
\Gamma &= e^{i\frac{2\pi}{\sqrt{3}}}\left(\cos\left(\frac{\pi}{\sqrt{2}}\right) - i\sqrt{\frac{3}{8}}\sin\left(\frac{\pi}{\sqrt{2}}\right)\right),
\end{aligned}$$

and it may be verified that U'_1 reduces to U_1 in the limit that $J'_a, J'_b, J'_c, J'_d \rightarrow 0$. The U'_1 gate, like the U_1 gate, is applied at the beginning of the controlled-phase gate sequence, and hence acts on the computational basis states. By comparing the explicit matrix representations (32) and (34) it is clear that the crucial difference between U'_1 and U_1 is the appearance of the χ_+ terms on the diagonal of U'_1 (the difference between Ω and λ is irrelevant: it translates into a global phase). In order for U'_1 to act like U_1 , i.e., in order for it not to prepare a superposition of code states and the first four non-code states, χ_+ must vanish. Consulting the expression (33) for χ_+ , it is evident that this leads to a complicated transcendental equation relating the constants J'_a, J'_b, J'_d (but not involving J'_c). A numerical solution of the condition $\chi_+ = 0$ leads to the result that the constants J'_a, J'_b, J'_d can take on an infinite set of rationally related values. Upon setting the ratio J'_b/J'_d to any rational number (except 1), there is a corresponding rational value of J'_a .

Summary of Conditions

Summing up our findings, we have the following sufficient set of conditions for the modified gate sequence

$$CP' = U_1^{\dagger} \left[U_2^{\dagger} U_3^{\dagger} \right] U_5^{\dagger} U'_6(J'_B) U'_5 [U'_3(J'_3) U'_2(J'_2)] U'_1(J'_a, J'_b, J'_c, J'_d)$$

to work as a controlled-phase gate in the presence of four-body interactions:

1. The constant J'_c can take on an arbitrary value.

2. The constants J'_2 and J''_2 must be chosen to satisfy the transcendental equation $\eta = 0$.
3. The constants J'_3 and J''_3 must be chosen to satisfy the transcendental equation $\eta = 0$.
4. The constant J'_5 must either be zero or chosen such that Λ is an even integer (i.e. $\sqrt{\frac{4}{3}(J'_5)^2 - 2J'_5 + 1}$ is an even integer).
5. The constant J'_B must be an integer.
6. The constants J'_a, J'_b, J'_d can take on an infinite set of rationally related values, where the ratio of any pair (e.g., J'_b/J'_d) can be chosen completely arbitrarily, and the value of the third constant is determined by this choice.

The most restrictive of these conditions is that J'_B must be an integer. However, note that since the gates are applied sequentially, this condition need only be satisfied during the application of the U'_6 gate, and it is plausible from the earlier sections of this paper that corresponding Heisenberg exchange constants can be found. When these conditions are satisfied it is indeed the case that $CP' = (-1, 1, 1, 1)$ on the code space.

Dimensionality of Parameter Spaces Required by Two-Body and Four-Body Couplings

We caution that, although the encoding procedure described above has been shown mathematically to remove the effect of the four-body couplings, the experimental construction of a suitable apparatus using real quantum dots is another matter, as the following heuristic calculation suggests.

Our modified gates imply the following constraints on the coupling coefficients:

U'_5 gate

- (a) $K_2[FG] = \frac{1}{2}K_2[GH]$;
- (b) Either $K_2[FH] = 0$, or $\Lambda(K_2[FH]) = 2n$, where n must have an integer value;

U'_B gate

- (c) $K_2[ij]$ is the same for all pairs within $\{A, B, C, D\}$;
- (d) $K_4[ABCD] = K_4[ACBD] = K_4[ADBC]$;
- (e) $K_4[ABCD] = 2mK_2[AB]$, where m may have any integer value;

U'_2 gate

- (f) $K_2[FG] = K_2[FH] = K_2[GH]$;
- (g) $K_2[EF] = \frac{3}{2}K_2[GH]$;

- (h) $K_4[EGFH] = K_4[EHFG]$;
- (i) Either $K_4[EFHG] = K_4[EGFH]$, or $K_4[EFHG]$ and $K_4[EGFH]$ satisfy the transcendental equation $\eta(K_4[EFHG], K_4[EGFH]) = 0$;

U'_3 gate

- (j) $K_2[AB] = K_2[AC] = K_2[BC]$;
- (k) $K_2[CD] = \frac{3}{2}K_2[AB]$;
- (l) $K_4[ACBD] = K_4[ADBC]$;
- (m) Either $K_4[ABCD] = K_4[ACBD]$, or $K_4[ABCD]$ and $K_4[ACBD]$ satisfy the transcendental equation $\eta(K_4[ABCD], K_4[ACBD]) = 0$;

U'_1 gate

- (n) $K_2[ij]$ is the same for all pairs within $\{A, B, C, D\}$;
- (o) $K_2[DE] = 2K_2[AB]$;
- (p) $K_4[ABCD] = K_4[ACBD] = K_4[ADBC]$;
- (q) $K_4[ABCE] = K_4[ACBE] = K_4[AEBCE]$;
- (r) $K_4[ADBE] = K_4[AEBD]$;
- (s) $K_4[ADCE] = K_4[AECD]$;
- (t) $K_4[BDCE] = K_4[BECD]$;
- (u) $K_4[ADBE] = K_4[ADCE] = K_4[BDCE]$;
- (v) $K_4[ABDE]$ is a single-valued function of $K_4[ADBE]$;
- (w) $K_4[BCDE]$ is a single-valued function of $K_4[ADCE]$;
- (x) $K_4[ACDE]$ is a single-valued function of $K_4[BDCE]$.

Since the coupling coefficients must in general vary with time in order to satisfy all of these constraints (for example, $K_2[CD]$ and $K_2[AC]$ would be equal during the operation of U'_B , but unequal during U'_3), we also assume that particular constraints need to be concurrently satisfied only when they arise from the same gate.

First, by the same reasoning used to derive Eqs. (6) and (23), we note that a four-dot Hamiltonian for the geometry of $\{A, B, C, E\}$ contains a constant term and 9 independent coupling coefficients. If these 9 coefficients take on a given set of values and we wish to adjust them to meet constraints such as those listed above, we would need 9 additional degrees of freedom in the system. We make the conservative assumption, however, that one two-body coefficient and one four-body coefficient can be left unaltered and the others adjusted to correspond

to them, which means that only 7 additional parameters are required. Similarly, for the subset $\{A, B, D, E\}$ ($\{A, C, D, E\}$, $\{B, C, D, E\}$, $\{A, B, C, D\}$), there are 9 (6, 7, 5) independent coupling coefficients, for which we require 7 (4, 5, 3) tunable parameters if a given set of constraints are to be satisfied. Of course, we will count one more degree of freedom whenever a constraint includes relationships between the two-body and four-body energies.

Now suppose that we designate one “base” choice of $\{x_b, x_c, x_v\}$, such that within each of the two squares, all the quantities $K_2[ij]$ are equal, all the quantities $K_4[ijkl]$ are equal, and $K_4[ijkl] = 2K_2[ij]$. That arrangement can simultaneously satisfy constraints (b), (c), (d), (e), (f), (h), (i), (j), (l), (m), (n), and (p), provided that the value of $K_2[FH]$ is chosen appropriately. From this potential, we would need to make one change within $\{E, F, G, H\}$ to reach condition (a) or condition (g), or one change within $\{5, 6, 7, 8\}$ to obtain (k) or (o). The couplings of $\{A, B, C, E\}$ must be adjusted to match (q) while still satisfying (n), (o), and (p), which requires 6 additional degrees of freedom as explained in the previous paragraph. Similarly, (v) ((w), (x)) and (r) ((s), (t)) together imply particular adjustments to the four-body couplings in $\{A, B, D, E\}$ ($\{A, C, D, E\}$, $\{B, C, D, E\}$), which requires 6 (3,4) new parameters. (The single-valued function in question is the same for all three cases, so $K_4[ABDE]$ ends up equalling $K_4[ACDE]$ and $K_4[BCDE]$.) Finally, we need two more degrees of freedom available somewhere in order to meet constraint (u), for a grand total of 28 degrees of freedom.

To put the size of this number into perspective, we will also count the independently tuned energies necessary to meet the conditions on EQC using pairwise couplings alone. By choosing a suitable combination of $\{x_b, x_c, x_v\}$ for an entire eight-spin system, we could satisfy (b), (c), (f), (j), and (n) at the same time; one more degree of freedom would be necessary to also satisfy (o). Starting from such a system, we could presumably satisfy (a) or (g) by adjusting one parameter within $\{E, F, G, H\}$, or satisfy (k) by adjusting one parameter within $\{A, B, C, D\}$. Hence we estimate that 7 degrees of freedom are required for the purely Heisenberg Hamiltonian used in Ref. [29]. We see that, even if one presupposes the ability to create and position many identical qubits of the form (28), (29) (3 free parameters), accounting correctly for two-body and four-body coupling is still a great deal more demanding than two-body coupling alone. It is this experimental challenge that must be weighed against the increased length (and hence vulnerability to decoherence) of pulse sequences employing only two-body couplings [30].

SUMMARY AND CONCLUSIONS

Earlier work [17, 32] showed that in highly symmetrical geometries, the interaction between three and four

mutually interacting electrons confined in parabolic potentials contains many-body terms, which in the case of four electrons qualitatively modify the usual Heisenberg interaction. In this work we have improved upon these early results by considering realistic, linear and square geometries, and by utilizing Gaussian confining potentials. Specifically, we have shown in a Heitler-London calculation that in the case of four mutually interacting electrons, in both the linear and square geometries, the system’s Hamiltonian contains four-body exchange terms which may be of comparable strength to the Heisenberg exchange interactions. This can have important implications for quantum information processing using coupled quantum dots. We have considered, in particular, the implications for the quantum computing using logical qubits encoded into decoherence-free subspaces of four electrons per qubit. We showed that previously designed conditional quantum logic gates between these encoded qubits must be modified, in order to account for the four-body terms that alter the (previously assumed) Heisenberg interaction, when four or more electrons are coupled simultaneously. This requires the ability to tune, to a certain extent, the four-body exchange constants. It is worth noting, however, that there are alternatives to this method of implementing encoded conditional logic gates, which may be less demanding. In particular, it is worth exploring the possibility of completing the set of universal encoded quantum logic gates by supplementing single-qubit gates (where, as we have shown, four-body effects are harmless) with measurements and teleportation, as in linear optics quantum computing [40]. This will be a subject for future research.

ACKNOWLEDGMENTS

A.M. and R.W. acknowledge the support of the Packard Foundation. D.A.L. acknowledges support under the DARPA-QuIST program (managed by AFOSR under agreement No. F49620-01-1-0468), and the Sloan Foundation. R.W. is grateful to Dr. Rusko Ruskov for constructive discussion.

APPENDIX: CALCULATION OF EXCHANGE COEFFICIENTS FOR THE FOUR-DOT SYSTEM

Equation (22) defines the computational basis for our system of four electrons confined by the potential (21). The Clebsch-Gordan method applied to dots A and C , then to dots B and D , and finally to the two pairs of dots, produces the orthogonal basis

$$\begin{aligned}
|2\ 2; 1\ 1\rangle &= |\Psi(\uparrow\uparrow\uparrow\uparrow)\rangle \\
|2\ 1; 1\ 1\rangle &= \frac{1}{2} [|\Psi(\uparrow\uparrow\uparrow\downarrow)\rangle + |\Psi(\uparrow\uparrow\downarrow\uparrow)\rangle + |\Psi(\uparrow\downarrow\uparrow\uparrow)\rangle + |\Psi(\downarrow\uparrow\uparrow\uparrow)\rangle] \\
|2\ 0; 1\ 1\rangle &= \frac{1}{\sqrt{6}} [|\Psi(\uparrow\uparrow\downarrow\downarrow)\rangle + |\Psi(\uparrow\downarrow\uparrow\downarrow)\rangle + |\Psi(\uparrow\downarrow\downarrow\uparrow)\rangle + |\Psi(\downarrow\uparrow\uparrow\downarrow)\rangle + |\Psi(\downarrow\uparrow\downarrow\uparrow)\rangle + |\Psi(\downarrow\downarrow\uparrow\uparrow)\rangle] \\
|2\ -1; 1\ 1\rangle &= \frac{1}{2} [|\Psi(\uparrow\downarrow\downarrow\downarrow)\rangle + |\Psi(\downarrow\uparrow\downarrow\downarrow)\rangle + |\Psi(\downarrow\downarrow\uparrow\downarrow)\rangle + |\Psi(\downarrow\downarrow\downarrow\uparrow)\rangle] \\
|2\ -2; 1\ 1\rangle &= |\Psi(\downarrow\downarrow\downarrow\downarrow)\rangle \\
|1\ 1; 1\ 1\rangle &= \frac{1}{2} [|\Psi(\uparrow\uparrow\uparrow\downarrow)\rangle - |\Psi(\uparrow\uparrow\downarrow\uparrow)\rangle + |\Psi(\uparrow\downarrow\uparrow\uparrow)\rangle - |\Psi(\downarrow\uparrow\uparrow\uparrow)\rangle] \\
|1\ 0; 1\ 1\rangle &= \frac{1}{\sqrt{2}} [|\Psi(\uparrow\downarrow\uparrow\downarrow)\rangle - |\Psi(\downarrow\uparrow\downarrow\uparrow)\rangle] \\
|1\ -1; 1\ 1\rangle &= \frac{1}{2} [|\Psi(\uparrow\downarrow\downarrow\downarrow)\rangle - |\Psi(\downarrow\uparrow\downarrow\downarrow)\rangle + |\Psi(\downarrow\downarrow\uparrow\downarrow)\rangle - |\Psi(\downarrow\downarrow\downarrow\uparrow)\rangle] \\
|0\ 0; 1\ 1\rangle &= |\Psi(\uparrow\downarrow\uparrow\downarrow)\rangle - \frac{1}{2} [|\Psi(\uparrow\uparrow\downarrow\downarrow)\rangle + |\Psi(\uparrow\downarrow\downarrow\uparrow)\rangle + |\Psi(\downarrow\uparrow\uparrow\downarrow)\rangle + |\Psi(\downarrow\downarrow\uparrow\uparrow)\rangle] + |\Psi(\downarrow\uparrow\downarrow\uparrow)\rangle \\
|1\ 1; 1\ 0\rangle &= \frac{1}{\sqrt{2}} [|\Psi(\uparrow\uparrow\uparrow\downarrow)\rangle - |\Psi(\uparrow\downarrow\uparrow\uparrow)\rangle] \\
|1\ 0; 1\ 0\rangle &= \frac{1}{2} [|\Psi(\uparrow\uparrow\downarrow\downarrow)\rangle - |\Psi(\uparrow\downarrow\downarrow\uparrow)\rangle + |\Psi(\downarrow\uparrow\uparrow\downarrow)\rangle - |\Psi(\downarrow\downarrow\uparrow\uparrow)\rangle] \\
|1\ -1; 1\ 0\rangle &= \frac{1}{\sqrt{2}} [|\Psi(\downarrow\uparrow\downarrow\downarrow)\rangle - |\Psi(\downarrow\downarrow\downarrow\uparrow)\rangle] \\
|1\ 1; 0\ 1\rangle &= \frac{1}{\sqrt{2}} [|\Psi(\uparrow\uparrow\downarrow\uparrow)\rangle - |\Psi(\downarrow\uparrow\uparrow\uparrow)\rangle] \\
|1\ 0; 0\ 1\rangle &= \frac{1}{2} [|\Psi(\uparrow\uparrow\downarrow\downarrow)\rangle + |\Psi(\uparrow\downarrow\downarrow\uparrow)\rangle - |\Psi(\downarrow\uparrow\uparrow\downarrow)\rangle - |\Psi(\downarrow\downarrow\uparrow\uparrow)\rangle] \\
|1\ -1; 0\ 1\rangle &= \frac{1}{\sqrt{2}} [|\Psi(\uparrow\downarrow\downarrow\downarrow)\rangle - |\Psi(\downarrow\uparrow\downarrow\downarrow)\rangle] \\
|0\ 0; 0\ 0\rangle &= \frac{1}{2} [|\Psi(\uparrow\uparrow\downarrow\downarrow)\rangle - |\Psi(\uparrow\downarrow\downarrow\uparrow)\rangle - |\Psi(\downarrow\uparrow\uparrow\downarrow)\rangle + |\Psi(\downarrow\downarrow\uparrow\uparrow)\rangle]
\end{aligned}$$

(the four indices on the left-hand side are S_T , $S_{T,z}$, $|\mathbf{S}_A + \mathbf{S}_C|$, and $|\mathbf{S}_B + \mathbf{S}_D|$). We need to choose five distinct combinations of good quantum numbers in order to write down five independent equations for our coupling coefficients; we shall use $((\mathbf{S}_A + \mathbf{S}_C)^2, \mathbf{S}_B + \mathbf{S}_D)^2, S_T^2) \in (2, 2, 6), (2, 2, 2), (2, 2, 0), (2, 0, 2), (0, 0, 0)$. (The combination $(0, 2, 2)$ is redundant, because a cyclic permutation of the labels A, B, C, D turns those states into the $(2, 0, 2)$ states without altering their energies.) Putting the relevant eigenfunctions into the left-hand side of (10) yields

$$\begin{aligned}
\frac{\langle 2\ 2; 1\ 1 | H_{\text{spin}} | 2\ 2; 1\ 1 \rangle}{\langle 2\ 2; 1\ 1 | 2\ 2; 1\ 1 \rangle} &= L_0 + 6L_1 + 4L'_1 \\
&\quad + 36L_2 + 4L'_2 \quad (35) \\
\frac{\langle 1\ 1; 1\ 1 | H_{\text{spin}} | 1\ 1; 1\ 1 \rangle}{\langle 1\ 1; 1\ 1 | 1\ 1; 1\ 1 \rangle} &= L_0 + 2L_1 + 4L'_1 + 4L_2 + 4L'_2 \\
\frac{\langle 1\ 1; 1\ 0 | H_{\text{spin}} | 1\ 1; 1\ 0 \rangle}{\langle 1\ 1; 1\ 0 | 1\ 1; 1\ 0 \rangle} &= L_0 + 2L_1 + 2L'_1 + 4L_2 \\
\frac{\langle 0\ 0; 1\ 1 | H_{\text{spin}} | 0\ 0; 1\ 1 \rangle}{\langle 0\ 0; 1\ 1 | 0\ 0; 1\ 1 \rangle} &= L_0 + 4L'_1 + 4L'_2 \\
\frac{\langle 0\ 0; 0\ 0 | H_{\text{spin}} | 0\ 0; 0\ 0 \rangle}{\langle 0\ 0; 0\ 0 | 0\ 0; 0\ 0 \rangle} &= L_0;
\end{aligned}$$

the corresponding energies are

$$\begin{aligned}
E_{2,2;1,1} &= \frac{\langle \Psi(\uparrow\uparrow\uparrow\uparrow) | H | \Psi(\uparrow\uparrow\uparrow\uparrow) \rangle}{\langle \Psi(\uparrow\uparrow\uparrow\uparrow) | \Psi(\uparrow\uparrow\uparrow\uparrow) \rangle} \\
E_{1,1;1,1} &= \frac{\langle \Psi(\uparrow\uparrow\uparrow\downarrow) | H | \Psi(\uparrow\uparrow\uparrow\downarrow) \rangle - 2\langle \Psi(\uparrow\uparrow\uparrow\downarrow) | H | \Psi(\uparrow\uparrow\downarrow\uparrow) \rangle + \langle \Psi(\uparrow\uparrow\uparrow\downarrow) | H | \Psi(\uparrow\downarrow\uparrow\uparrow) \rangle}{\langle \Psi(\uparrow\uparrow\uparrow\downarrow) | \Psi(\uparrow\uparrow\uparrow\downarrow) \rangle - 2\langle \Psi(\uparrow\uparrow\uparrow\downarrow) | \Psi(\uparrow\uparrow\downarrow\uparrow) \rangle + \langle \Psi(\uparrow\uparrow\uparrow\downarrow) | \Psi(\uparrow\downarrow\uparrow\uparrow) \rangle} \\
E_{1,0;1,0} &= \frac{\langle \Psi(\uparrow\uparrow\downarrow\downarrow) | H | \Psi(\uparrow\uparrow\downarrow\downarrow) \rangle - \langle \Psi(\uparrow\uparrow\downarrow\downarrow) | H | \Psi(\downarrow\downarrow\uparrow\uparrow) \rangle}{\langle \Psi(\uparrow\uparrow\downarrow\downarrow) | \Psi(\uparrow\uparrow\downarrow\downarrow) \rangle - \langle \Psi(\uparrow\uparrow\downarrow\downarrow) | \Psi(\downarrow\downarrow\uparrow\uparrow) \rangle} \\
E_{0,0;1,1} &= [\langle \Psi(\uparrow\uparrow\downarrow\downarrow) | H | \Psi(\uparrow\uparrow\downarrow\downarrow) \rangle - 8\langle \Psi(\uparrow\uparrow\downarrow\downarrow) | H | \Psi(\uparrow\downarrow\uparrow\downarrow) \rangle + 2\langle \Psi(\uparrow\uparrow\downarrow\downarrow) | H | \Psi(\uparrow\downarrow\downarrow\uparrow) \rangle + \langle \Psi(\uparrow\uparrow\downarrow\downarrow) | H | \Psi(\downarrow\downarrow\uparrow\uparrow) \rangle \\
&\quad + 2\langle \Psi(\uparrow\downarrow\uparrow\downarrow) | H | \Psi(\uparrow\downarrow\uparrow\downarrow) \rangle + 2\langle \Psi(\uparrow\downarrow\uparrow\downarrow) | H | \Psi(\downarrow\uparrow\downarrow\uparrow) \rangle] / [\langle \Psi(\uparrow\uparrow\downarrow\downarrow) | \Psi(\uparrow\uparrow\downarrow\downarrow) \rangle - 8\langle \Psi(\uparrow\uparrow\downarrow\downarrow) | \Psi(\uparrow\downarrow\uparrow\downarrow) \rangle \\
&\quad + 2\langle \Psi(\uparrow\uparrow\downarrow\downarrow) | \Psi(\uparrow\downarrow\uparrow\downarrow) \rangle + \langle \Psi(\uparrow\uparrow\downarrow\downarrow) | \Psi(\downarrow\downarrow\uparrow\uparrow) \rangle + 2\langle \Psi(\uparrow\downarrow\uparrow\downarrow) | \Psi(\uparrow\downarrow\uparrow\downarrow) \rangle + 2\langle \Psi(\uparrow\downarrow\uparrow\downarrow) | \Psi(\downarrow\uparrow\downarrow\uparrow) \rangle] \\
E_{0,0;0,0} &= \frac{\langle \Psi(\uparrow\uparrow\downarrow\downarrow) | H | \Psi(\uparrow\uparrow\downarrow\downarrow) \rangle - 2\langle \Psi(\uparrow\uparrow\downarrow\downarrow) | H | \Psi(\uparrow\downarrow\downarrow\uparrow) \rangle + \langle \Psi(\uparrow\uparrow\downarrow\downarrow) | H | \Psi(\downarrow\downarrow\uparrow\uparrow) \rangle}{\langle \Psi(\uparrow\uparrow\downarrow\downarrow) | \Psi(\uparrow\uparrow\downarrow\downarrow) \rangle - 2\langle \Psi(\uparrow\uparrow\downarrow\downarrow) | \Psi(\uparrow\downarrow\downarrow\uparrow) \rangle + \langle \Psi(\uparrow\uparrow\downarrow\downarrow) | \Psi(\downarrow\downarrow\uparrow\uparrow) \rangle}.
\end{aligned} \tag{36}$$

Again we take inner products over the spin degrees of freedom to obtain

$$\begin{aligned}
\langle \Psi(\uparrow\uparrow\uparrow\uparrow) | H | \Psi(\uparrow\uparrow\uparrow\uparrow) \rangle &= 24[H_I - 4H_I - 2H_{\setminus} + 8H_{\Delta} + 2H_{||} + H_{\times} - 2H_{\diamond} - 4H_{\bowtie}] \\
\langle \Psi(\uparrow\uparrow\uparrow\downarrow) | H | \Psi(\uparrow\uparrow\uparrow\downarrow) \rangle &= 24[H_I - 2H_I - H_{\setminus} + 2H_{\Delta}] \\
\langle \Psi(\uparrow\uparrow\uparrow\downarrow) | H | \Psi(\uparrow\uparrow\downarrow\uparrow) \rangle &= 24[-H_I + 2H_{\Delta} + H_{||} - H_{\diamond} - H_{\bowtie}] \\
\langle \Psi(\uparrow\uparrow\uparrow\downarrow) | H | \Psi(\uparrow\downarrow\uparrow\uparrow) \rangle &= 24[-H_{\setminus} + 2H_{\Delta} + H_{\times} - 2H_{\bowtie}] \\
\langle \Psi(\uparrow\uparrow\downarrow\downarrow) | H | \Psi(\uparrow\uparrow\downarrow\downarrow) \rangle &= 24[H_I - 2H_I + H_{||}] \\
\langle \Psi(\uparrow\uparrow\downarrow\downarrow) | H | \Psi(\uparrow\downarrow\uparrow\downarrow) \rangle &= 24[-H_I + 2H_{\Delta} - H_{\bowtie}] \\
\langle \Psi(\uparrow\uparrow\downarrow\downarrow) | H | \Psi(\uparrow\downarrow\downarrow\uparrow) \rangle &= 24[-H_{\setminus} + 2H_{\Delta} - H_{\diamond}] \\
\langle \Psi(\uparrow\uparrow\downarrow\downarrow) | H | \Psi(\downarrow\downarrow\uparrow\uparrow) \rangle &= 24[H_{||} + H_{\times} - 2H_{\bowtie}] \\
\langle \Psi(\uparrow\downarrow\uparrow\downarrow) | H | \Psi(\uparrow\downarrow\uparrow\downarrow) \rangle &= 24[H_I - 2H_{\setminus} + H_{\times}] \\
\langle \Psi(\uparrow\downarrow\uparrow\downarrow) | H | \Psi(\downarrow\uparrow\downarrow\uparrow) \rangle &= 24[2H_{||} - 2H_{\diamond}],
\end{aligned} \tag{37}$$

where

$$\begin{aligned}
H_I &\equiv \langle ABCD | H | ABCD \rangle \\
H_I &\equiv \langle ABCD | H | ABDC \rangle \\
H_{\setminus} &\equiv \langle ABCD | H | ADCB \rangle \\
H_{\Delta} &\equiv \langle ABCD | H | ADBC \rangle \\
H_{||} &\equiv \langle ABCD | H | BADC \rangle \\
H_{\times} &\equiv \langle ABCD | H | CDAB \rangle \\
H_{\diamond} &\equiv \langle ABCD | H | DABC \rangle \\
H_{\bowtie} &\equiv \langle ABCD | H | BDAC \rangle
\end{aligned} \tag{38}$$

(again, the pictorial subscripts indicate the geometry of each orbital exchange), and

$$\begin{aligned}
\langle \Psi(\uparrow\uparrow\uparrow\uparrow) | \Psi(\uparrow\uparrow\uparrow\uparrow) \rangle &= 24[1 - 4\langle A | B \rangle^2 - 2\langle A | C \rangle^2 + 8\langle A | B \rangle^2 \langle A | C \rangle + \langle A | C \rangle^4 - 4\langle A | B \rangle^2 \langle A | C \rangle^2] \quad (39) \\
\langle \Psi(\uparrow\uparrow\uparrow\downarrow) | \Psi(\uparrow\uparrow\uparrow\downarrow) \rangle &= 24[1 - 2\langle A | B \rangle^2 - \langle A | C \rangle^2 + 2\langle A | B \rangle^2 \langle A | C \rangle] \\
\langle \Psi(\uparrow\uparrow\uparrow\downarrow) | \Psi(\uparrow\uparrow\downarrow\uparrow) \rangle &= 24[-\langle A | B \rangle^2 + 2\langle A | B \rangle^2 \langle A | C \rangle - \langle A | B \rangle^2 \langle A | C \rangle^2] \\
\langle \Psi(\uparrow\uparrow\uparrow\downarrow) | \Psi(\uparrow\downarrow\uparrow\uparrow) \rangle &= 24[-\langle A | C \rangle^2 + 2\langle A | B \rangle^2 \langle A | C \rangle + \langle A | C \rangle^4 - 2\langle A | B \rangle^2 \langle A | C \rangle^2] \\
\langle \Psi(\uparrow\uparrow\downarrow\downarrow) | \Psi(\uparrow\uparrow\downarrow\downarrow) \rangle &= 24[1 - 2\langle A | B \rangle^2 + \langle A | B \rangle^4] \\
\langle \Psi(\uparrow\uparrow\downarrow\downarrow) | \Psi(\uparrow\downarrow\uparrow\downarrow) \rangle &= 24[-\langle A | B \rangle^2 + 2\langle A | B \rangle^2 \langle A | C \rangle - \langle A | B \rangle^2 \langle A | C \rangle^2] \\
\langle \Psi(\uparrow\uparrow\downarrow\downarrow) | \Psi(\uparrow\downarrow\downarrow\uparrow) \rangle &= 24[-\langle A | C \rangle^2 + 2\langle A | B \rangle^2 \langle A | C \rangle - \langle A | B \rangle^4] \\
\langle \Psi(\uparrow\uparrow\downarrow\downarrow) | \Psi(\downarrow\downarrow\uparrow\uparrow) \rangle &= 24[\langle A | B \rangle^4 + \langle A | C \rangle^4 - 2\langle A | B \rangle^2 \langle A | C \rangle^2] \\
\langle \Psi(\uparrow\downarrow\uparrow\downarrow) | \Psi(\uparrow\downarrow\uparrow\downarrow) \rangle &= 24[1 - 2\langle A | C \rangle^2 + \langle A | C \rangle^4] \\
\langle \Psi(\uparrow\downarrow\uparrow\downarrow) | \Psi(\downarrow\uparrow\downarrow\uparrow) \rangle &= 0.
\end{aligned}$$

The following one-body integrals are needed to evaluate the overlap terms (39) and the energies (38):

$$\begin{aligned}
\langle A | A \rangle &= 1 \\
\langle A | h | A \rangle &= \frac{\hbar\omega_o}{2048} [945x_b^{-3} + 5600x_b^{-2} + 7360x_b^{-1} + 4608] \\
\langle A | B \rangle &= e^{-x_b} \\
\langle A | h | B \rangle &= \frac{\hbar\omega_o}{2048} [945x_b^{-3} + 3080x_b^{-2} + 2376x_b^{-1} + 2272 - 624x_b] e^{-x_b} \\
\langle A | C \rangle &= e^{-2x_b} \\
\langle A | h | C \rangle &= \frac{\hbar\omega_o}{2048} [945x_b^{-3} + 560x_b^{-2} + 416x_b^{-1} + 1792 - 1792x_b] e^{-2x_b}
\end{aligned} \quad (40)$$

for the quadratic potential, and

$$\begin{aligned}
\langle A | A \rangle &= 1 \\
\langle A | h | A \rangle &= \hbar\omega_o \left\{ \frac{3}{4} - \frac{x_v^{5/2} e^{-\frac{2x_b(p+1)^2}{x_v+1}} \left(e^{\frac{4px_b}{x_v+1}} + 1 \right)^2}{2(x_v+1)^{3/2}} \right\} \\
\langle A | B \rangle &= e^{-p^2 x_b} \\
\langle A | h | B \rangle &= \hbar\omega_o \left\{ \left(\frac{3}{4} - \frac{p^2 x_b}{2} \right) e^{-p^2 x_b} - \frac{x_v^{5/2} e^{-\frac{(p^2 x_v + 2p^2 + 2p+2)x_b}{x_v+1}} \left(1 + e^{\frac{4px_b}{x_v+1}} \right)}{(x_v+1)^{3/2}} \right\} \\
\langle A | C \rangle &= e^{-2p^2 x_b} \\
\langle A | h | C \rangle &= \hbar\omega_o \left\{ \left(\frac{3}{4} - p^2 x_b \right) e^{-2p^2 x_b} - \frac{2x_v^{5/2} e^{-2x_b(p^2 + \frac{1}{x_v+1})}}{(x_v+1)^{3/2}} \right\}
\end{aligned}$$

for the exponential potential, where the parameter p now reflects a shift of all four localized orbital wave functions

toward the square's center in order to minimize their one-

body energies: $p = 1$ means no change from Fig. 7, and $p = 0$ would mean that all four orbitals overlapped entirely. (The two-body formula (17) remains the same, since it is independent of both V and N .) Combining Eqs. (17), (24), and (35) - (40), we obtain the coefficients K_0 , $K_2[AB]$, $K_2[AC]$, $K_4[ABCD]$, and $K_4[ACBD]$.

-
- [1] D. Loss and D.P. DiVincenzo, Phys. Rev. A 57, 120 (1998).
 - [2] M.A. Nielsen and I.L. Chuang, Quantum Computation and Quantum Information (Cambridge University Press, Cambridge, U.K., 2000) 191-193.
 - [3] J. Preskill, Proc. Roy. Soc. Lond. A 454, 385-410 (1998).
 - [4] R. Raussendorf and H.J. Briegel, Phys. Rev. Lett. 86, 5188 (2001), quant-ph/0010033.
 - [5] D. Bacon, J. Kempe, D.A. Lidar and K.B. Whaley, Phys. Rev. Lett. 85, 1758 (2000), quant-ph/9909058.
 - [6] J. Kempe, D. Bacon, D.A. Lidar, and K.B. Whaley, Phys. Rev. A 63, 042307 (2001), quant-ph/0004064.
 - [7] D.P. DiVincenzo, D. Bacon, J. Kempe, G. Burkard, and K.B. Whaley, Nature 408, 339 (2000).
 - [8] D. Bacon, J. Kempe, D.P. DiVincenzo, D.A. Lidar, and K.B. Whaley, in Proceedings of the 1st International Conference on Experimental Implementations of Quantum Computation, Sydney, Australia, edited by R. Clark (Rinton, Princeton, NJ, 2001), p. 257, quant-ph/0102140.
 - [9] D.A. Lidar and L.-A. Wu, Phys. Rev. Lett. 88, 017905 (2002), quant-ph/0109021.
 - [10] D. Bacon, K.R. Brown, K.B. Whaley, Phys. Rev. Lett. 87, 247902 (2001), quant-ph/0012018.
 - [11] E. Farhi, J. Goldstone, S. Gutmann, J. Lapan, A. Lundgren, D. Preda, Science 292, 472 (2001).
 - [12] P.W. Shor, in Proceedings of the 37th Symposium on Foundations of Computing (IEEE Computer Society Press, Los Alamitos, CA, 1996), p. 56, quant-ph/9605011.
 - [13] D. Gottesman, Phys. Rev. A 57, 127 (1997).
 - [14] A.M. Steane, Nature 399, 124 (1999).
 - [15] D.A. Lidar, D. Bacon, J. Kempe, and K.B. Whaley, Phys. Rev. A 63, 022307 (2001).
 - [16] M.H. Freedman, Commun. Math. Phys. 234, 129 (2003).
 - [17] A. Mizel and D.A. Lidar, Phys. Rev. Lett. 92, 077903 (2004).
 - [18] F.R. Waugh, M.J. Berry, C.H. Crouch, C. Livermore, D.J. Mar, R.M. Westervelt, K.L. Campman, and A.C. Gossard, Phys. Rev. B 53, 1413 (1996).
 - [19] G. Burkard, H.-A. Engel and D. Loss, Fortschr. Phys. 48, 965 (2000).
 - [20] X. Hu and S. Das Sarma, Phys. Rev. A 61, 062301 (2000).
 - [21] V.W. Scarola, K. Park, and S. Das Sarma, Phys. Rev. Lett. 93, 120503 (2004).
 - [22] V.W. Scarola and S. Das Sarma, Phys. Rev. A 71, 032340 (2005).
 - [23] P. Zanardi, Phys. Rev. A 60, R729 (1999), quant-ph/9901047.
 - [24] L.-A. Wu and D.A. Lidar, Phys. Rev. Lett. 88, 207902 (2002), quant-ph/0112144.
 - [25] L.-A. Wu, M.S. Byrd, D.A. Lidar, Phys. Rev. Lett. 89, 127901 (2002), quant-ph/0202168.
 - [26] P. Zanardi and M. Rasetti, Phys. Rev. Lett. 79, 3306 (1997), quant-ph/9705044.
 - [27] D.A. Lidar, D. Bacon, J. Kempe and K.B. Whaley, Phys. Rev. A 61, 052307 (2000), quant-ph/9907096.
 - [28] D.A. Lidar, K.B. Whaley, Decoherence-Free Subspaces and Subsystems (2003), quant-ph/0301032.
 - [29] D.M. Bacon, Ph.D. thesis, Univ. of California, Berkeley (2001), available at <http://www.cs.caltech.edu/~dabacon/research>.
 - [30] M. Hsieh, J. Kempe, S. Myrgren, K.B. Whaley, Q. Inf. Processing 2, 289 (2004).
 - [31] W. Heitler and F. London, Z. Physik 44, 455 (1927).
 - [32] A. Mizel and D.A. Lidar, Phys. Rev. B 70, 115310 (2004).
 - [33] G. Burkard, D. Loss and D.P. DiVincenzo, Phys. Rev. B 59, 2070 (1999), cond-mat/9808026.
 - [34] X. Hu and S. Das Sarma, Phys. Rev. A 64, 042312 (2001), cond-mat/0101102.
 - [35] J. Levy, Phys. Rev. Lett. 89, 147902 (2002), quant-ph/0101057.
 - [36] J. Levy, Oxide-Semiconductor Materials for Quantum Computation (2002), quant-ph/0209008.
 - [37] R. de Sousa and S. Das Sarma, Phys. Rev. B 68, 115322 (2003).
 - [38] E. Yablonovitch, H.W. Jiang, H. Kosaka, H.D. Robinson, D.S. Rao, and T. Szkopek, Proc. of the IEEE 91, 761 (2003).
 - [39] A. Barenco, C.H. Bennett, R. Cleve, D.P. DiVincenzo, N. Margolus, P. Shor, T. Sleator, J. Smolin and H. Weinfurter, Phys. Rev. A 52, 3457 (1995).
 - [40] E. Knill, R. Laflamme, and G. J. Milburn, Nature 409, 46 (2001).
 - [41] All matrix calculations reported here were performed with Mathematica.

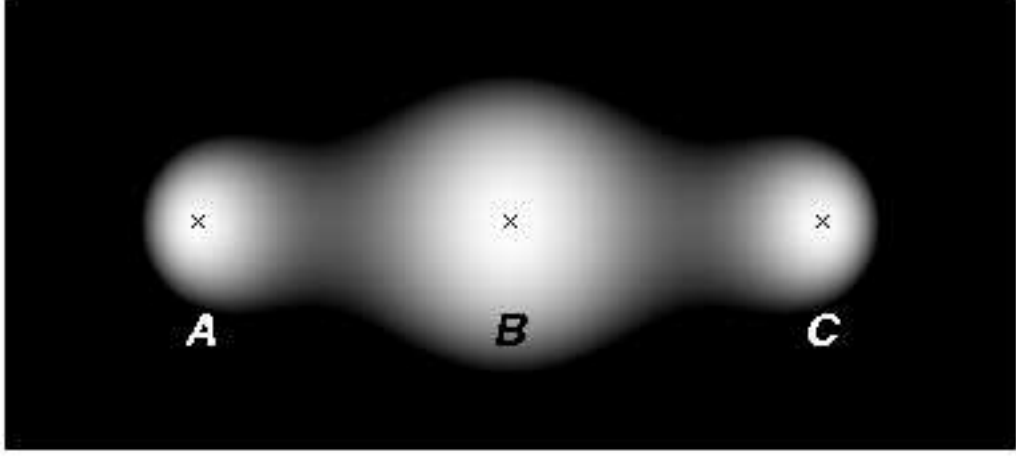


FIG. 1: Simple model of three collinear quantum dots using quadratic minima. The potential (3) depends on three spatial variables; this is its cross-section in the x - y plane, with $x_b = 1$. Dark areas indicate regions of high potential.



FIG. 2: Probability density of the localized orbital state $\phi_A(\mathbf{r})$ for three quantum wells arranged in a linear geometry. In this plot $x_b = 1$. Dark regions indicate large values of $|\phi_A|^2$.

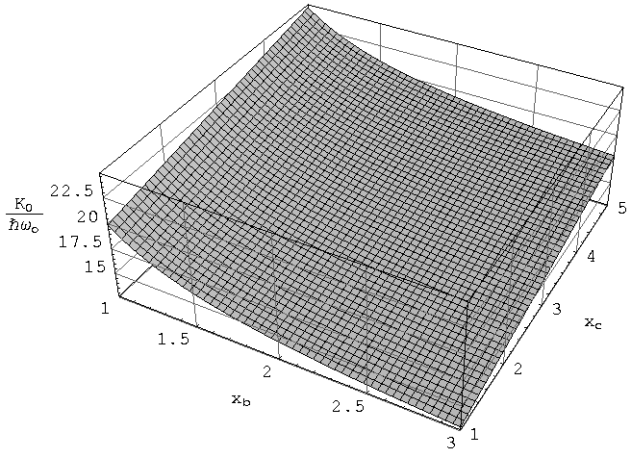


FIG. 3: Plot of K_0 , the overall energy shift, as a function of dimensionless barrier height x_b and Coulomb energy x_c in the case of three mutually interacting electrons in a linear geometry.

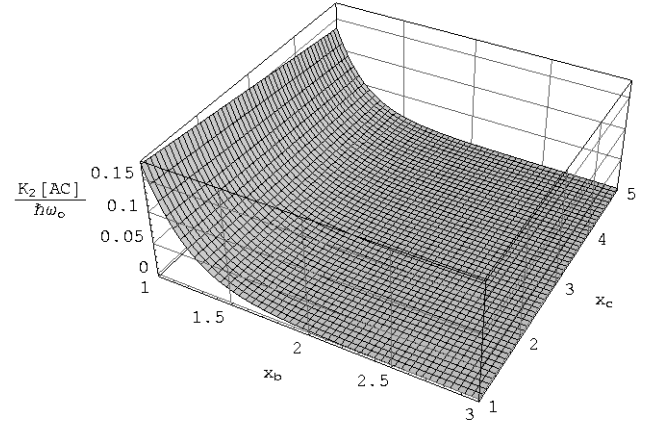


FIG. 5: Plot of $K_2[AC]$, the two-body coupling coefficient for non-adjacent dots, as a function of dimensionless barrier height x_b and Coulomb energy x_c in the case of three mutually interacting electrons in a linear geometry.

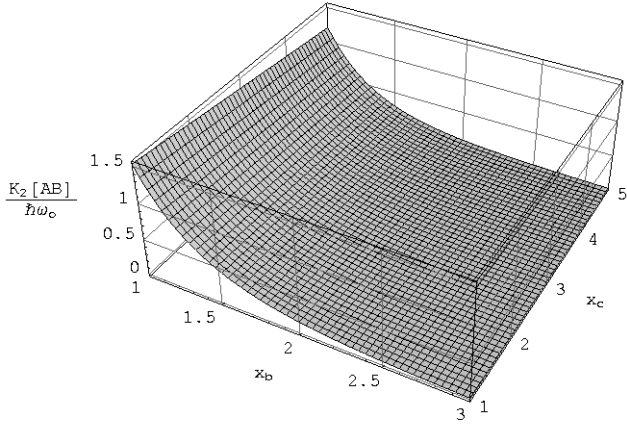


FIG. 4: Plot of $K_2[AB]$, the two-body coupling coefficient for adjacent dots, as a function of dimensionless barrier height x_b and Coulomb energy x_c in the case of three mutually interacting electrons in a linear geometry.

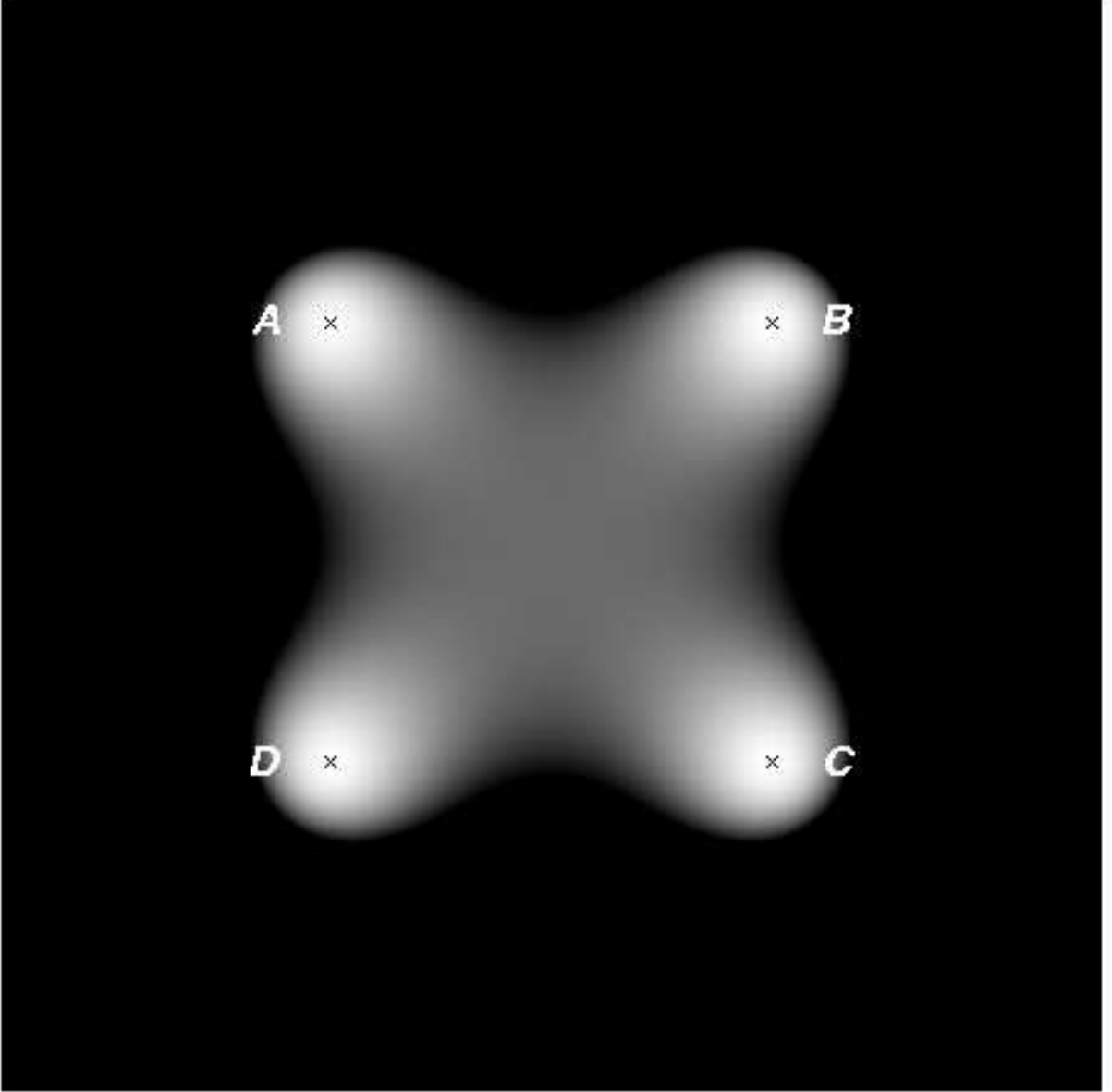


FIG. 6: Simple model of four quantum dots arranged in a square geometry, using quadratic minima. The potential (21) depends on three spatial variables; this is its cross-section in the x - y plane, with $x_b = 1$. Dark areas indicate regions of high potential.

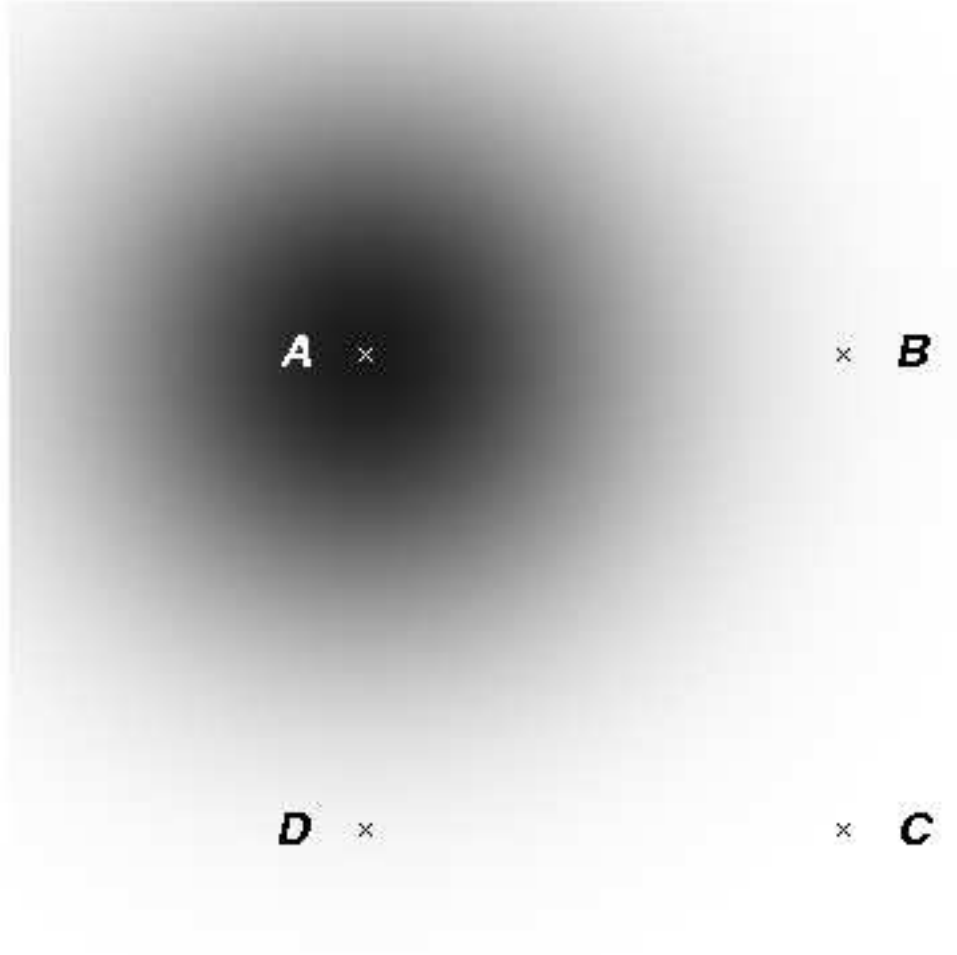


FIG. 7: Probability density of the localized orbital state $\phi_A(\mathbf{r})$ for four quantum wells arranged in a square geometry. In this plot $x_b = 1$. Dark regions indicate large values of $|\phi_A|^2$.

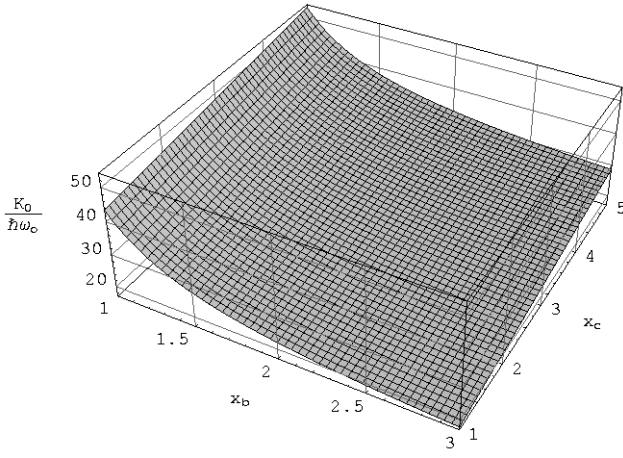


FIG. 8: Plot of K_0 , the overall energy shift, as a function of dimensionless barrier height x_b and Coulomb energy x_c in the case of four mutually interacting electrons in a square geometry.

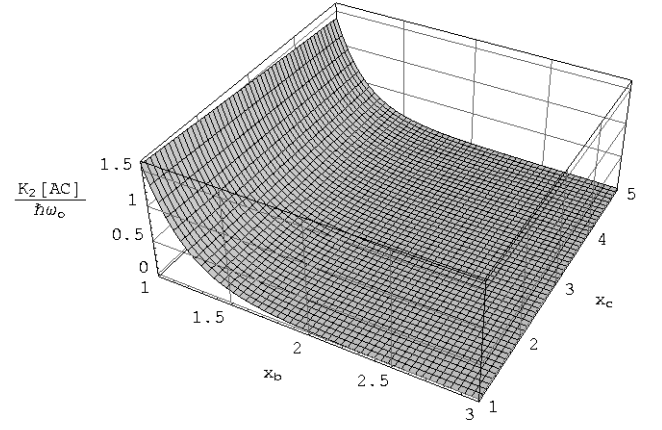


FIG. 10: Plot of $K_2[AC]$, the two-body coupling coefficient for non-adjacent dots, as a function of dimensionless barrier height x_b and Coulomb energy x_c in the case of four mutually interacting electrons in a square geometry.

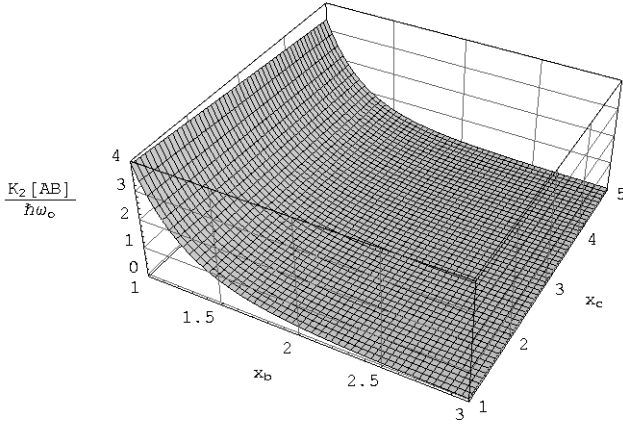


FIG. 9: Plot of $K_2[AB]$, the two-body coupling coefficient for adjacent dots, as a function of dimensionless barrier height x_b and Coulomb energy x_c in the case of four mutually interacting electrons in a square geometry.

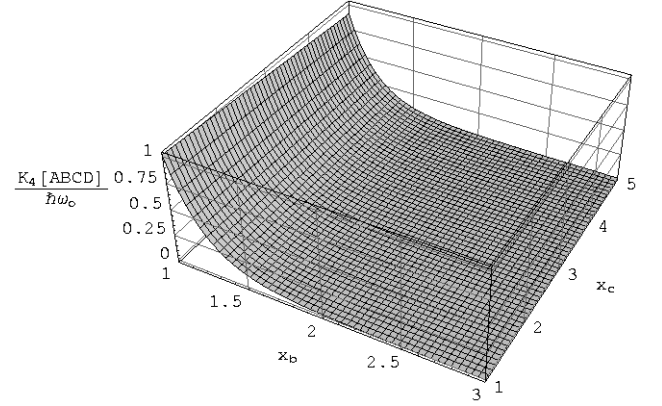


FIG. 11: Plot of $K_4[ABCD]$, the four-body coupling coefficient for pairs of adjacent dots, as a function of dimensionless barrier height x_b and Coulomb energy x_c in the case of four mutually interacting electrons in a square geometry.

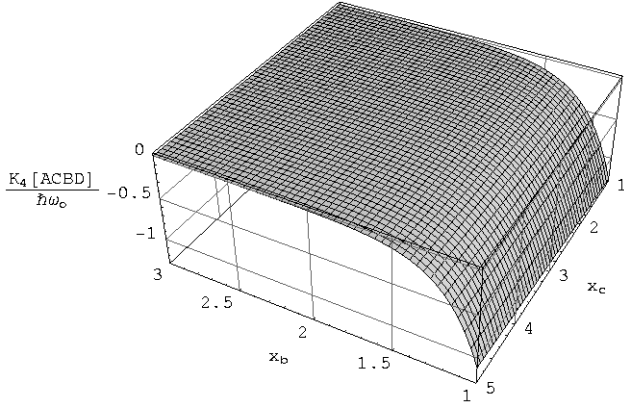


FIG. 12: Plot of $K_4[ACBD]$, the four-body coupling coefficient for pairs of non-adjacent dots, as a function of dimensionless barrier height x_b and Coulomb energy x_c in the case of four mutually interacting electrons in a square geometry. Note that two of the axis directions are reversed from the preceding figures.

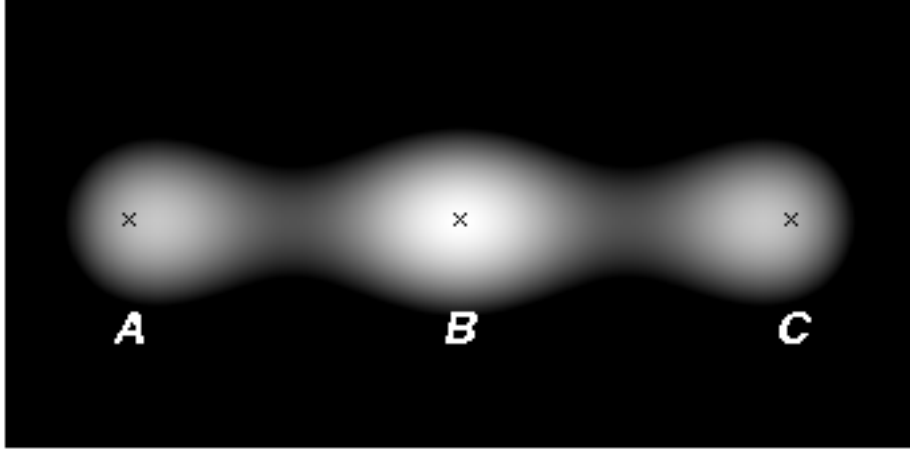


FIG. 13: Simple model of three collinear quantum dots using overlapping Gaussian minima. The potential (3) depends on three spatial variables; this is its cross-section in the x - y plane, with $x_b = \frac{5}{2}$ and $x_v = \frac{7}{2}$. Dark areas indicate regions of high potential.

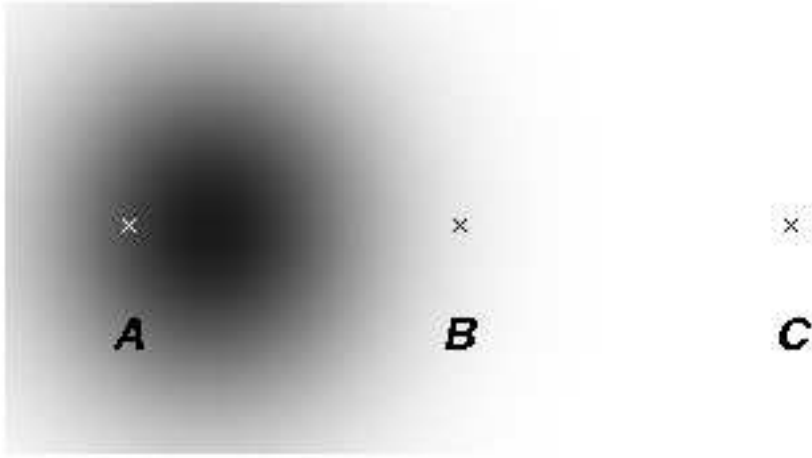


FIG. 14: Probability density of the localized orbital state $\phi_A(\mathbf{r})$ for three quantum wells arranged in a linear geometry. In this plot $x_b = \frac{5}{2}$, $x_v = \frac{7}{2}$. Dark regions indicate large values of $|\phi_A|^2$. The center of the wave function has been shifted so that its average energy is minimized, to better approximate the (unknown) true orbital eigenstate.

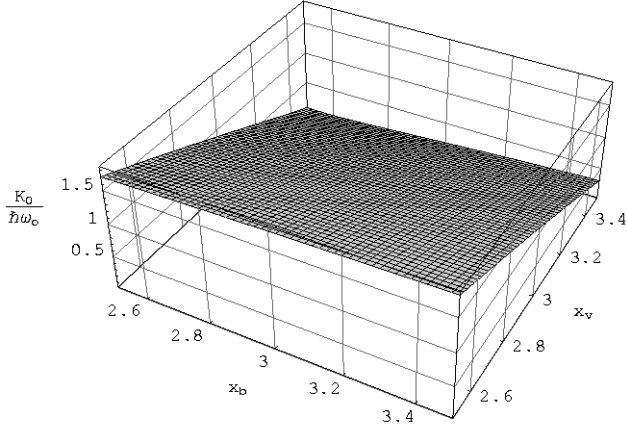


FIG. 15: Plot of K_0 , the overall energy shift, as a function of dimensionless barrier height x_b and overall well depth x_v in the case of three mutually interacting electrons in a linear geometry. In this and succeeding figures, the Coulomb repulsion parameter x_c is set to 1.5 as in Ref. [17].

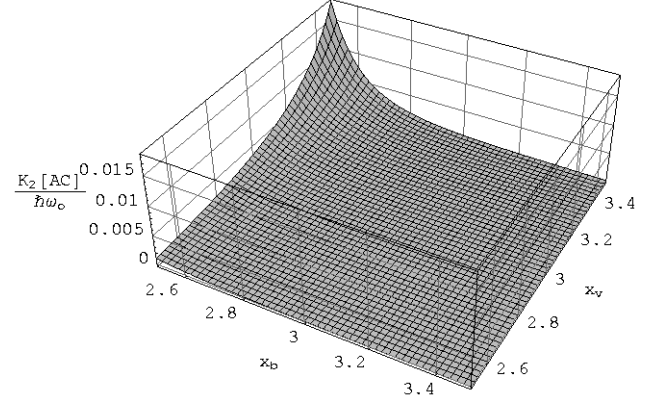


FIG. 17: Plot of $K_2[AC]$, the two-body coupling coefficient for non-adjacent dots, as a function of dimensionless barrier height x_b and overall well depth x_v in the case of three mutually interacting electrons in a linear geometry.

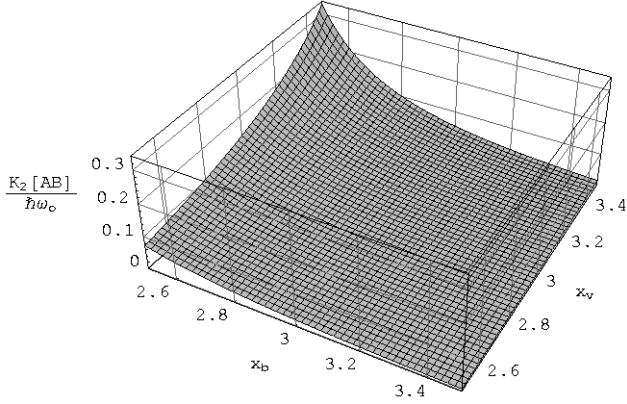


FIG. 16: Plot of $K_2[AB]$, the two-body coupling coefficient for adjacent dots, as a function of dimensionless barrier height x_b and overall well depth x_v in the case of three mutually interacting electrons in a linear geometry.

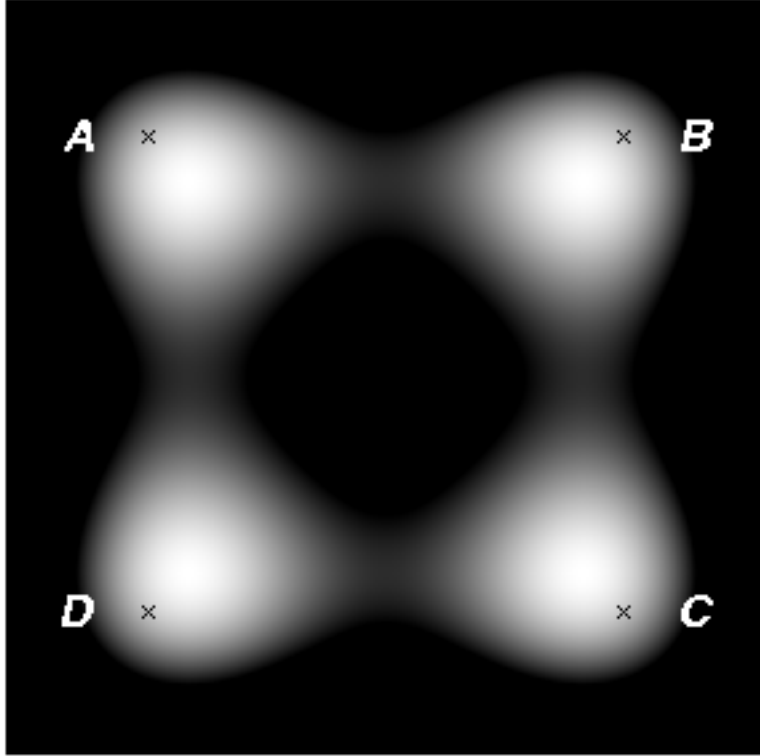


FIG. 18: Simple model of four quantum dots arranged in a square geometry, using overlapping Gaussian minima. The potential (21) depends on three spatial variables; this is its cross-section in the x - y plane, with $x_b = 1$. Dark areas indicate regions of high potential.

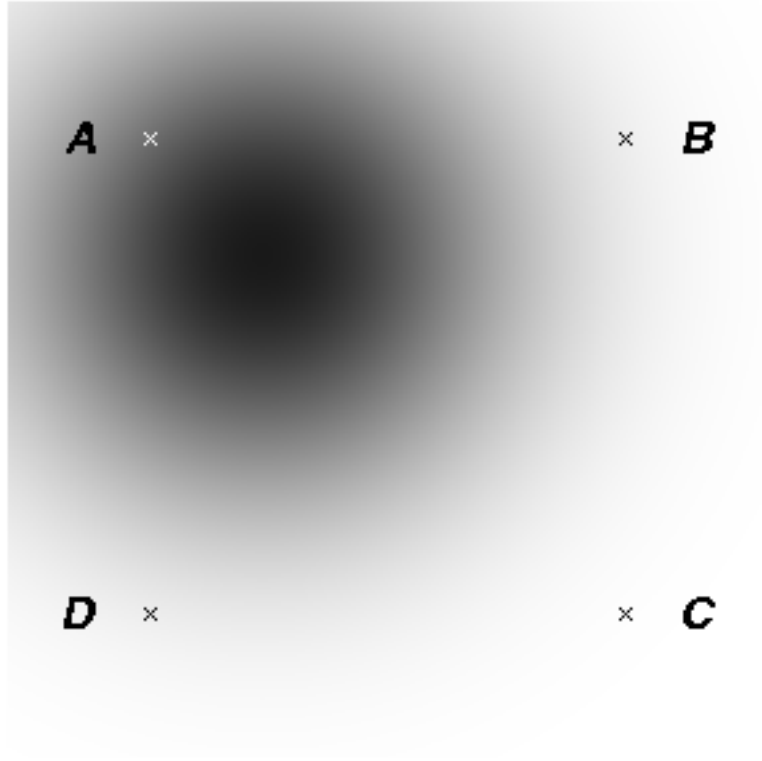


FIG. 19: Probability density of the localized orbital state $\phi_A(\mathbf{r})$ for three quantum wells arranged in a linear geometry. In this plot $x_b = \frac{5}{2}$, $x_v = \frac{7}{2}$. Dark regions indicate large values of $|\phi_A|^2$. The center of the wave function has been shifted so that its average energy is minimized, to better approximate the (unknown) true orbital eigenstate.

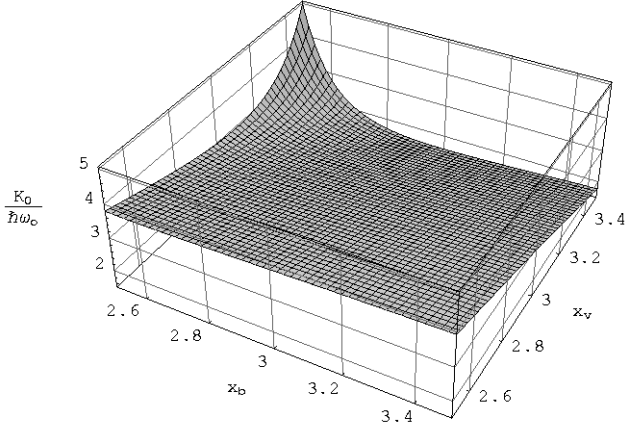


FIG. 20: Plot of K_0 , the overall energy shift, as a function of dimensionless barrier height x_b and overall well depth x_v in the case of four mutually interacting electrons in a square geometry.

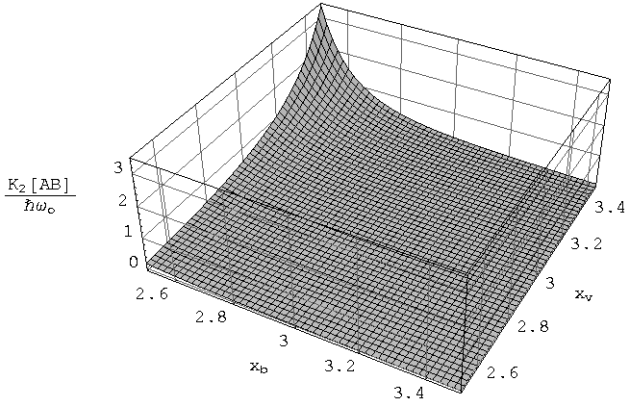


FIG. 21: Plot of $K_2[AB]$, the two-body coupling coefficient for adjacent dots, as a function of dimensionless barrier height x_b and overall well depth x_v in the case of four mutually interacting electrons in a square geometry.

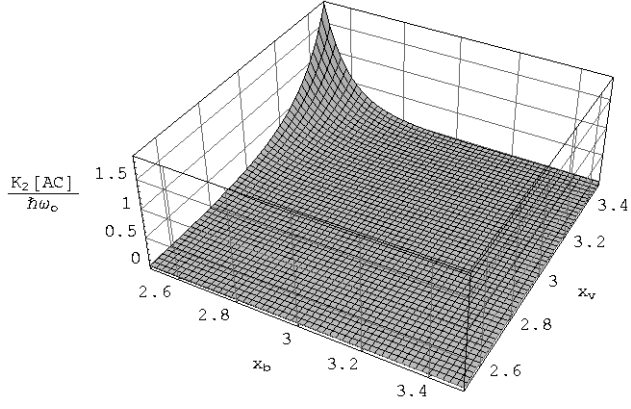


FIG. 22: Plot of $K_2[AC]$, the two-body coupling coefficient for non-adjacent dots, as a function of dimensionless barrier height x_b and overall well depth x_v in the case of four mutually interacting electrons in a square geometry.

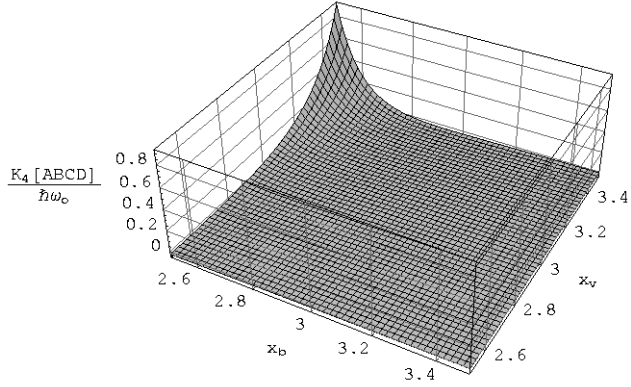


FIG. 23: Plot of $K_4[ABCD]$, the four-body coupling coefficient for pairs of adjacent dots, as a function of dimensionless barrier height x_b and overall well depth x_v in the case of four mutually interacting electrons in a square geometry.

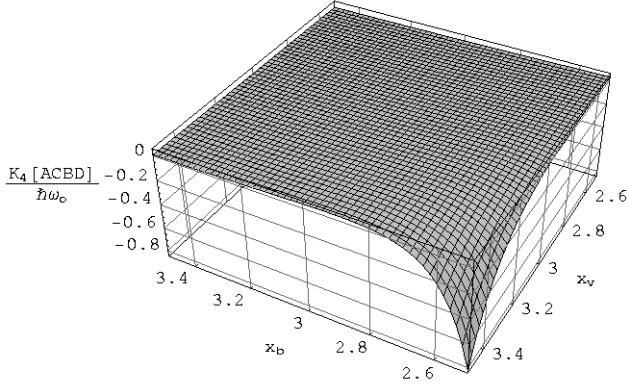


FIG. 24: Plot of $K_4[ACBD]$, the four-body coupling coefficient for pairs of non-adjacent dots, as a function of dimensionless barrier height x_b and overall well depth x_v in the case of four mutually interacting electrons in a square geometry. Note that two of the axis directions are reversed from the preceding figures.

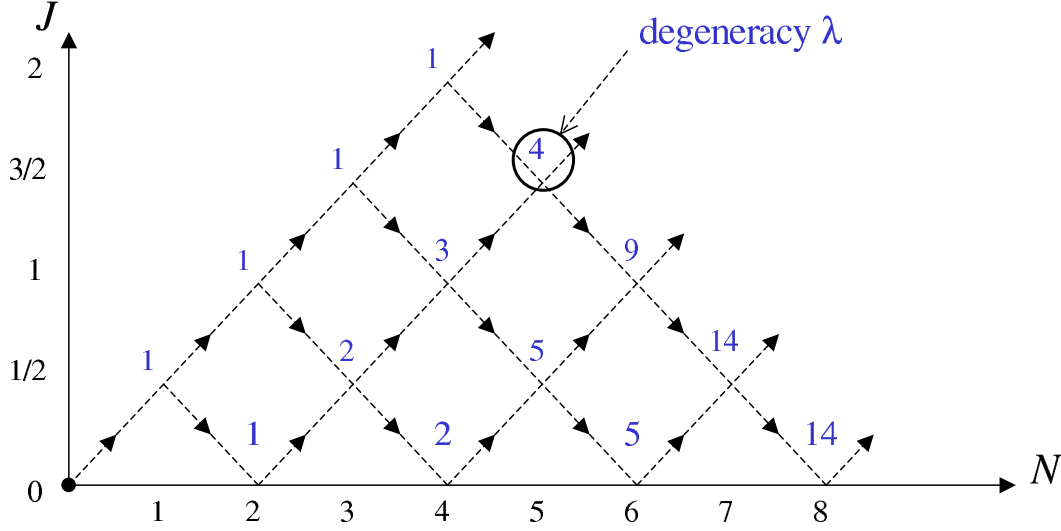


FIG. 25: Partitioning of the Hilbert space of N spin-1/2 particles into DF subspaces (nodes of the graph). The integer above each node represents the number of paths leading from the origin to that node.